Petroleum Science 20 (2023) 3654–3672

Contents lists available at ScienceDirect

Petroleum Science

journal homepage: www.keaipublishing.com/en/journals/petroleum-science

Original Paper

# Risk pre-assessment method for regional drilling engineering based on deep learning and multi-source data

Yu-Qiang Xu [a, b, *], Kuan Liu [a, b], Bao-Lun He [a, b], Tatiana Pinyaeva [a], Bing-Shuo Li [a, b], Yu-Cong Wang [a, b], Jia-Jun Nie [a, b], Lei Yang [a, b], Fu-Xiang Li [a, b]

[a] National Key Laboratory of Deep Oil and Gas, China University of Petroleum (East China), Qingdao, 266580, Shandong, China
[b] Shandong Ultra-Deep Drilling Process Control Tech RD Center, Qingdao, 266580, Shandong, China

ARTICLE INFO

*Article history:*
Received 11 July 2022
Received in revised form
13 June 2023
Accepted 13 June 2023
Available online 21 June 2023

Edited by Jia-Jia Fei

*Keywords:*
Pre-drill risk assessment
Risk samples
Deep learning
LSTM neural network
3D model

ABSTRACT

Accurately predicting downhole risk before drilling in new exploration areas is one of the difficulties. Using intelligent algorithms to explore the complex relationship between multi-source data and downhole risk is a hot research topic and frontier in this field. However, due to the small number and uneven distribution of drilled wells in new exploration areas and the lack of sample data related to risk, the training model has insufficient generalization ability, and thus the prediction is not effective. In this paper, a drilling risk profile (depth domain) rich in geological and engineering information is constructed by introducing a quantitative evaluation method for drilling risk of drilled wells, which can provide sufficient risk sample data for model training and thus solve the small sample problem. For the problem of uneven distribution of drilling wells in new exploration areas, the concept of virtual wells and their deployment methods were proposed. Besides, two methods for calculating rock mechanical parameters of virtual wells were proposed, and the accuracy and applicability of the two methods are analyzed. The LSTM deep learning model was optimized to tap the quantitative relationship between drilling risk profiles and multi-source data (e.g., seismic, logging, and rock mechanical parameters). The model was validated to have an average relative error of 9.19%. The quantitative prediction of the drilling risk profile of the virtual well was achieved using the trained LSTM model and the calculation of the relevant parameters of the virtual well. Finally, based on the sequential Gaussian simulation method and the risk distribution of drilled and virtual wells, a regional 3D drilling risk model was constructed. The analysis of real cases shows that the addition of virtual wells can significantly improve the identification of regional drilling risks and the prediction accuracy of pre-drill drilling risks in unexplored areas can be improved by up to 21% compared with the 3D risk model constructed based on drilled wells only.


## 1. Introduction

Currently, oil and gas exploration and development are advancing towards deep stratum and deep water (Sheng and Guan, 2019), but drilling in deep complex formations faces many challenges, such as strong uncertainty of formation information, prominent well control risks, and frequent occurrence of complex downhole accidents. In recent years, researchers have conducted extensive studies on pre-drilling risk prediction, during-drilling operation risk monitoring and risk-based decision-making optimization, by optimizing drilling engineering design through risk prediction before pre-drilling, identifying or warning risks in real-time during-drilling operation monitoring, and make optimization decisions quickly based on risk analysis. Due to the low pre-drill data and low awareness of deep formation information, and the sudden and often serious consequences of risks during drilling, most of the current research is focused on two aspects: drilling monitoring and decision optimization. For example, scholars from the Center for Risk, Integrity and Safety Engineering (C-RISE) at Memorial University of Newfoundland, Canada, have done a lot of research on monitoring the risk of well surge or blowout during drilling: Abimbola and Khan et al. (2016, 2018) proposed a dynamic risk analysis method based on loss function that changes with

* Corresponding author. College of Petroleum Engineering, China University of Petroleum (East China), Qingdao, 266580, Shandong, China.
*E-mail address:* z21020060@s.upc.edu.cn (Y.-Q. Xu).

https://doi.org/10.1016/j.petsci.2023.06.005

different well conditions and stages. The dynamic consequence model is established based on the loss function that constantly changes with the bottom pressure of the well, and is used to monitor and maintain the stability of the well at different stages; in addition, there are scholars who use a variety of downhole parameters to achieve the monitoring of well surge. For example, Rakibul Islam et al. (2017) used four parameters including downhole pressure, drilling mud density, mud conductivity and flow rate to monitor well surge, and through different logical combinations, achieved assessment of well surge and associated blowout risk. Based on these, Nhat et al. (2020) proposed a data-driven early monitoring of well surge based on a machine learning approach by introducing a Bayesian network and optimizing the former model. Sule et al. (2019) proposed a traditional Bayesian network by optimizing a dynamic blowout risk model based on dynamic Bayesian network that can monitor the risk situation during drilling in real time and validated in Amberjack filed in the Gulf of Mexico. For other risks such as well leakage monitoring, Unrau and Torrione (2017) established a well leakage judgment warning model based on real-time drilling data from multiple wells, and coupled a variety of machine learning methods to train "false alarm" and " failure alarm". During test, the false alarm rate for lost circulation was one in every 5 h, and the accuracy and reliability of pre-alarm were significantly improved. Alkinani et al. (2020) realized the prediction of lost circulation in natural fractures and induced fractures by creating two neural network models, dividing the data in each network model into three groups, and using ANN to continuously train and optimize the number of neurons, achieved the prediction of well leakage in natural and induced fractures, dividing the data in each network model into three groups, and optimizing the number of neurons using ANN training. In terms of decision optimization for risk, Alkinani et al. (2021) classified well leaks according to the degree of leakage, formation type, cost of leakage and success rate of plugging, and then set different expected expenditures of well leak management solutions based on decision tree algorithm and recommended the practically applicable and least expensive well leak solution based on different well leak incident types. Seraj et al. (2021) proposed a geospatial information system-assisted approach based on a soft computing, designed a framework for calculating the description of geological risk intervals and uncertainty estimation process for each hydrocarbon structure to manage the spatial uncertainty in the exploration process, and enhanced the risk analysis of the data-driven approach by a fuzzy logic approach, showing a high predictive capability. While drilling risks can be effectively reduced or even avoided through during-drilling monitoring and decision optimization, regulation during the drilling process (especially adjusting drilling engineering design schemes such as well structure) can increase non-operating time, while the ideal state of drilling engineering is to guarantee less or even no sudden risks during drilling through rational design, thus reducing non-operating time and increasing drilling time efficiency.

Therefore, a well-designed drilling engineering plan is crucial for safe and efficient drilling, especially in new exploration areas where there are few existing wells and limited reference data from adjacent wells. In such cases, a pre-assessment of downhole engineering risks is essential to develop a well-planned drilling engineering scheme that can minimize the risks associated with drilling encounters. By doing so, drilling operations can be conducted in a safer and more efficient manner. In recent years, scholars have proposed qualitative or semi-quantitative research methods such as Analytic Hierarchy Process (Li et al., 2018; He and Wang, 2010), Fault Tree Analysis (Yao et al., 2015), Interval Analysis (Guan et al., 2013), Tree Naive Bayes Algorithm-based modeling approach (Adedigba et al., 2018), Fuzzy Bow-tie Model Method (Liu et al., 2020), Monte Carlo simulation (Wei et al., 2013a, b; Zhao et al., 2019), and Mathematical statistics theory (Guan et al., 2009; Ke et al., 2009), which can be used to pre-drill the qualitative assessment of regional drilling engineering risks and the safety of engineering solutions. However, due to limitations in realistic factors and models, engineering practice has shown that qualitative or semi-quantitative methods may not fully meet the safety requirements of drilling engineering in complex formations (Sheng et al., 2019). In this regard, to address the problems of strong uncertainty of deep formation information and difficulty in quantitative evaluation of pre-drilling downhole engineering risks, Sheng et al. (2019) proposed a method to quantitatively characterize formation pressure uncertainty using credibility, and on this basis, constructed a quantitative evaluation method of downhole engineering risks such as lost circulation, kick, borehole collapse, and pipe sticking based on the wellbore pressure balance criterion, which can quantitatively assess the types and specific depths of complex occurrences in the well. The method has achieved good application results. However, the method relies on accurate formation pressure profiles and drilling construction plans, and is more suitable for post-evaluation of drilled wells, while for wells to be drilled, it is difficult to obtain accurate formation pressure and drilling construction plan information before drilling, which limits the application of the method in pre-drilling of wells to be drilled. Yi et al. (2021) used logging data from exploratory wells and drilling logs to obtain the rock mechanical properties and pressure profiles of neighboring wells, and then used the geomechanical profiles of multiple wells to establish a 3D geomechanical model of the entire block, which provided guidance for reducing drilling risks. However, this process only judges the risk based on well logging data and well history record data. To achieve quantitative evaluation, the graded risk level is generally classified using regional prediction approaches such as spatial difference to analyze the risk characteristics of the formation pressure system. Prediction results are affected by factors such as the accuracy of the risk grade of drilled wells and the uniformity of drilling spatial distribution. For new exploration areas, there are few and unevenly distributed drilled wells, and it is more difficult to obtain accurate prediction results. On the other hand, with the development of machine learning, artificial intelligence, and other technologies, the field of petroleum engineering is accelerating the crossover of disciplines, such as Liang et al. (2019), Jahanbakhshi et al. (2014), Zhang et al. (2022), Li et al. (2018), Xie et al. (2018), who proposed the optimization of support vector regression machine using particle swarm optimization algorithm, MLP algorithm, gradient boosting decision tree algorithm, random forest, BP neural network, etc. Such methods are based on various data before drilling to drive the model and use intelligent algorithms to construct complex relationships between various data and downhole risk to achieve quantitative assessment of drilling risk. However, these methods rely heavily on the number and quality of samples used for data training, and for a well or even a block, the risk specimens of downhole drilling engineering are small samples. For instance, there is only single risk information in the well history, such as specific well depths, events, and indirect monitoring data. The model obtained in this way is prone to overfitting to small samples and underfitting of task objectives, and it cannot guarantee the generalization ability of the model. Therefore, gaining sufficient quantity and quality of risk samples is one of the key bottlenecks of current data-driven risk assessment methods.

To solve the issues mentioned above, this paper proposes several solutions. First, using the drilled well engineering risk evaluation method based on the wellbore pressure balance criterion (Sheng et al., 2016) to construct a probabilistic profile of downhole engineering risk rich in geological and engineering

information, which can significantly improve the quantity and quality of risk samples. Second, construct quantitative relationships between seismic, formation lithology, physical properties, drilling parameters and downhole engineering risk profiles based on machine learning algorithms, add virtual wells in the undrilled area of the block, and use the quantitative relationships of drilled wells to quantitatively predict the downhole engineering risk profiles of virtual wells, thus solving the problem of few drilled wells and uneven spatial distribution in the new exploration area. Third, construct a regional three-dimensional risk model based on the downhole engineering risk profiles of drilled wells and virtual wells by using spatial difference and depth adjust methods. The three-dimensional risk model so constructed fully takes into account the influence of regional geology, engineering design and construction level, and is of great significance for improving the level of understanding of drilling engineering risks in deep complex formations before drilling, optimizing the engineering design plan of wells to be drilled, and reducing downhole engineering risks during drilling.

## 2. Quantitative risk assessment method of drilled engineering based on wellbore pressure balance criterion

### 2.1. Basic principle of method

In response to the problem of strong uncertainty of deep formation information and difficulty of quantitative evaluation of downhole engineering risks, Sheng et al. (2016, 2019) proposed a method of quantitative characterization of formation pressure uncertainty using credibility (pore pressure calculation of formation with credibility as an example, and its basic principle and effect are shown in Fig. 1, the specific principle is shown in Appendix I). Based on the wellbore pressure balance criterion, a quantitative evaluation method for downhole engineering risks such as lost circulation, kick, borehole collapse and pipe sticking is constructed, as presented in Eqs. (1)–(4) for the risk assessment model. This model can quantitatively evaluate the type and specific depth of downhole risk occurrence (i.e., the risk probability profile of downhole complex situations, as shown in Fig. 2). Field application has confirmed that the risk evaluation compliance rate of this method for drilled wells is greater than 92%. For more details, please refer to the literature (Sheng, 2019).

Since the method evaluates complex downhole situations based on the equilibrium relationship between formation pressure and wellbore pressure. As a result, its risk assessment results provides a wealth of geological information (such as formation pressure and its uncertainty) as well as engineering information (drilling mud density, wellbore structure scheme, construction level, etc.). Compared to the risk information recorded in well history (such as risk occurrence, well depth, surface monitoring overflow/lost circulation, etc.), the quantity and quality of samples used for data training are significantly enhanced.

The related risk evaluation model is as follows:

Kick $R_k$:

$$R_{k(h)} = P\left(\rho_d < \rho_{k(h)}\right) = 1 - F_{\rho_{k(b)}}(\rho_d) \tag{1}$$

Lost circulation $R_L$:

$$R_{L(h)} = P\left(\rho_d > \rho_{L(h)}\right) = F_{\rho_{L(b)}}(\rho_d) \tag{2}$$

Borehole collapse $R_{c(h)}$:

$$R_{c(h)} = \max\left\{P\left(\rho_d < \rho_{cl(h)}\right), P\left(\rho_d > \rho_{c2(h)}\right)\right\} = \max\left\{1 - F_{\rho_{c(b)}}(\rho_d), F_{\rho_{c2(b)}}(\rho_d)\right\} \tag{3}$$

Pipe sticking $R_{sk}$:

$$R_{sk(h)} = P\left(\rho_d < \rho_{sk(h)}\right) = F_{\rho_{sk(h)}}(\rho_d) \tag{4}$$

where $R_{k(h)}$, $R_{L(h)}$, $R_{c(h)}$ and $R_{sk(h)}$ represent kick, lost circulation, borehole collapse and pipe sticking at depth $h$, respectively; $\rho_d$ (g/cm$^3$) is the density of the drilling mud during drilling.

### 2.2. Analysis of drilling examples

This paper takes a block in the South China Sea is used as the research object, which is characteristics by ultra-high temperature, high pressure and narrow density window, and has drilled eight wells. Downhole complexities such as kick, lost circulation are common, and drilling risks are prominent. The distribution of the eight drilled wells in the seismic area is shown in Fig. 3.

Taking the drilled Well number 2 as an example. First, sort out the logging data used for calculation, and outliers were removed and noise reduction was performed on the data. The results are shown in Fig. 4.

The overburden pressure was calculated, and the pore pressure was calculated by using the effective stress method. The results are shown in Fig. 5.

In combination with the Eaton method, the Eaton index was inversely calculated and the probability distribution of the Eaton index was calculated. Combined with the probability distribution, the pore pressure with confidence was calculated. The fracture pressure and collapse pressure with credibility were calculated based on Monte Carlo simulation. The results are shown in Fig. 6.

Finally, based on the pressure equilibrium criterion, the density window of safe drilling mud with credibility was constructed, and the risk profile of Well number 2 was constructed based on the theory of generalized stress and strength interference.

Using the above method, we can obtain the risk profiles of eight drilled wells, as shown in Fig. 7.

In the future, dozens of development wells will be drilled in the seismic area shown in Fig. 3. However, as can be seen from the figure, the number of drilled wells in this seismic area is small and unevenly distributed. If the risk profile data of only eight drilled wells are used to evaluate the risk of regional drilling projects, it is difficult to fully reflect the overall situation of the block, especially when the development wells are located far away from the drilled wells, it is difficult for the existing technology to obtain a more accurate risk evaluation results. Therefore, this paper proposes the concept of virtual wells and its deployment method, by adding virtual wells to undrilled areas in the block, with a view to solving the problem of few drilled wells and uneven spatial distribution.

## 3. Determination method of virtual well location and related attributes

### 3.1. Determination method of virtual well location

It can be seen from Fig. 3, the distribution of drilled wells in the block is relatively scattered and there are large undrilled areas. If we rely only on the data of existing drilled wells, it is difficult to predict the risk characteristics of the whole block with high accuracy. Therefore, virtual wells need to be inserted in the undrilled

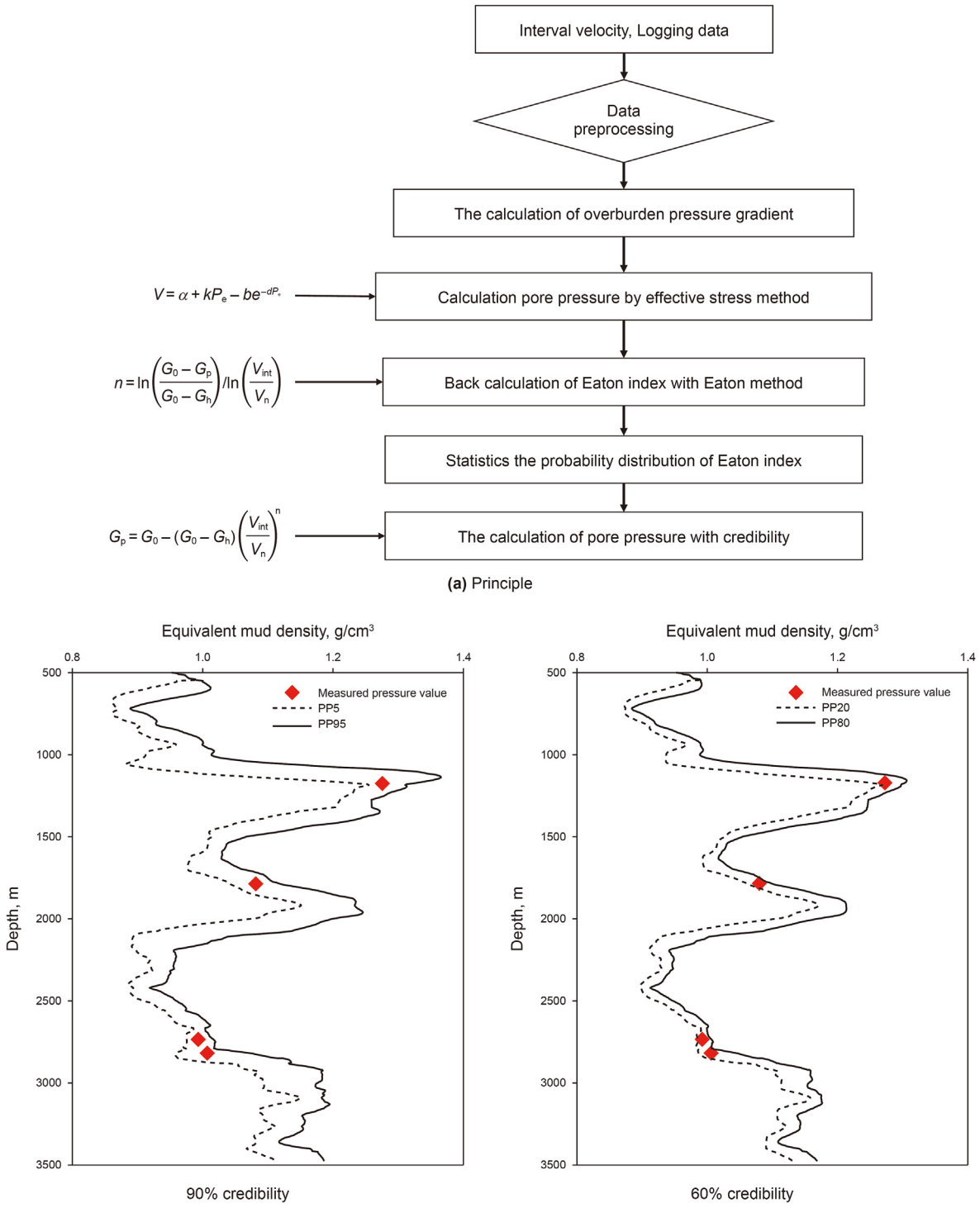


**Fig. 1.** Basic principle and effect of pore pressure calculation of formation with credibility (Ke, 2019).

area to enrich the block information and improve the prediction accuracy of the drilling risk of the whole block. To ensure that the selected virtual wells are randomly and uniformly distributed in the undrilled area, a random function (Wang and Li, 2014) was used to generate virtual wells:

The seismic plane region is denoted as $D = \{(x, y)|a \leqslant x \leqslant b, \varphi_1(x) \leqslant y \leqslant \varphi_2(x)\}$, then a point $(X, Y)$ in the region should obey the uniform distribution on the $D$ region, where the edge density function of $X$ is:

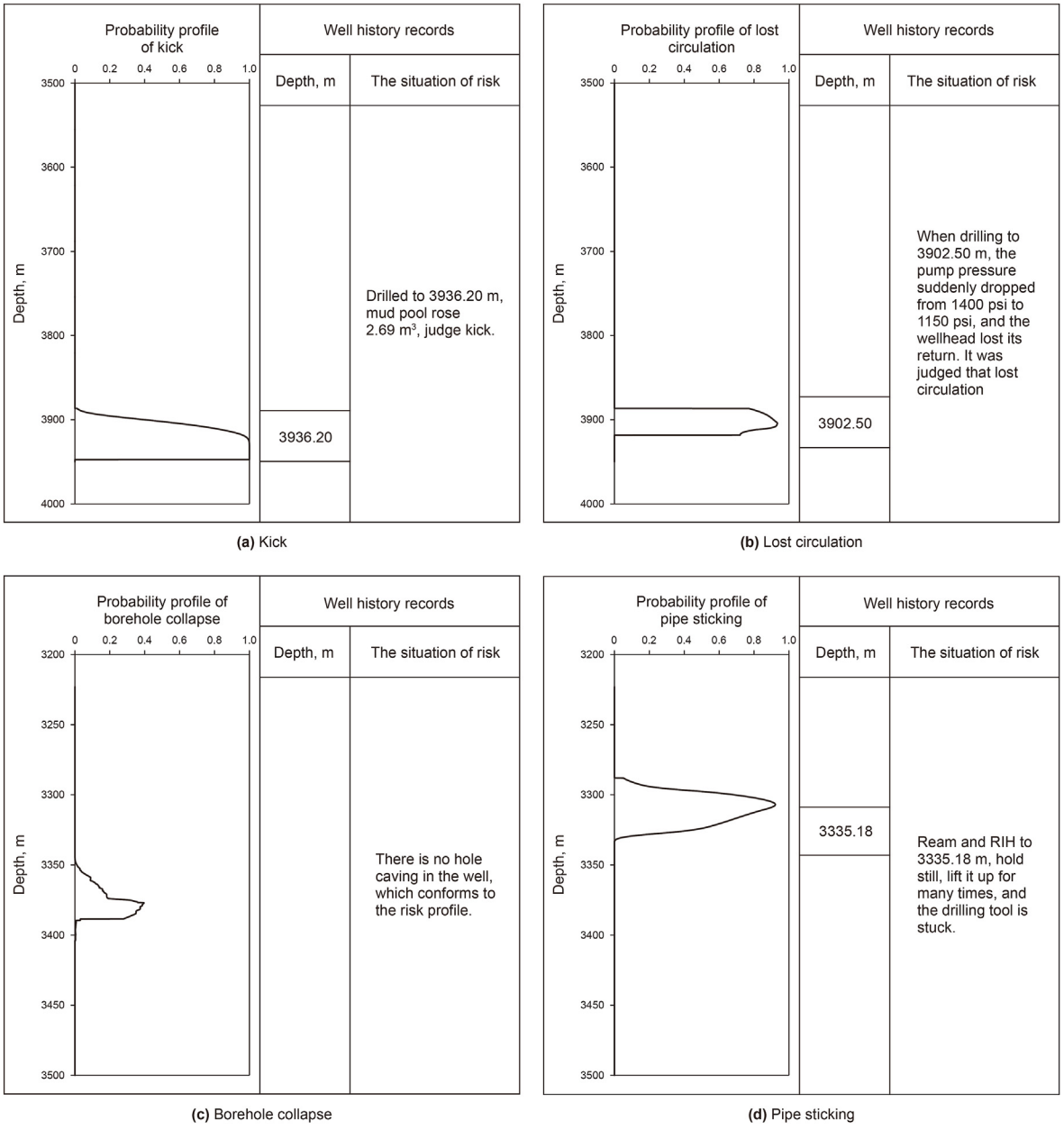


**Fig. 2.** Schematic diagram of the risk profile of the complex downhole situation in the well.

$$f_X(x)=\int_{-\infty}^{+\infty} f(x,y)\mathrm{d}y=\begin{cases}\int_{\varphi_1(x)}^{\varphi_2(x)}\left(\frac{1}{\iint_D \mathrm{d}\sigma}\right)\mathrm{d}y & a\leqslant x\leqslant \mathrm{b}\\ 0 \quad \text{others}\end{cases} \tag{5}$$

$$=\begin{cases}\frac{(\varphi_2(x)-\varphi_1(x))}{\iint_D \mathrm{d}\sigma \mathrm{d}y} & a\leqslant x\leqslant b\\ 0 \qquad \text{others}\end{cases}$$

where, $f_X(x)$ is the edge density function of $X$; $\varphi_2(x)$ and $\varphi_1(x)$ are the boundaries of seismic region.

Returns a random number $\xi$ in the interval $[0,1]$ by the random function Random. Assuming the mapping of $m$ from $\xi$ to $X$ is $X = m(\xi)$, and $m$ can be monotonically differentiable. Then, $f_\xi(g^{-1}(x))\cdot(m^{-1}(x))' = f_X(x)$ and $m(0) = a, m(1) = b$ , so it can be resolved:

$$\xi=\frac{\int_a^X(\varphi_2(u)-\varphi_1(u))\mathrm{d}u}{\int_a^b(\varphi_2(x)-\varphi_1(x))\mathrm{d}x} \tag{6}$$

where, $\xi$ is the value obtained by random function; $X$ is the X coordinate of the point to be solved; $a$ and $b$ are the boundaries of seismic region.

The value of $X$ can be obtained by substituting $\xi$. Again, $\eta$ can be obtained by the Random function, and $Y$ can be solved by the following formula.

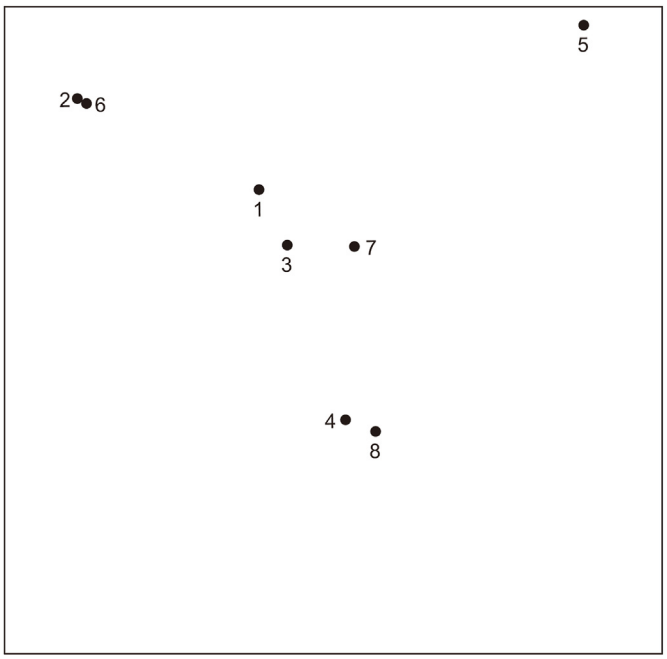


**Fig. 3.** Distribution map of drilled wells in the seismic area.

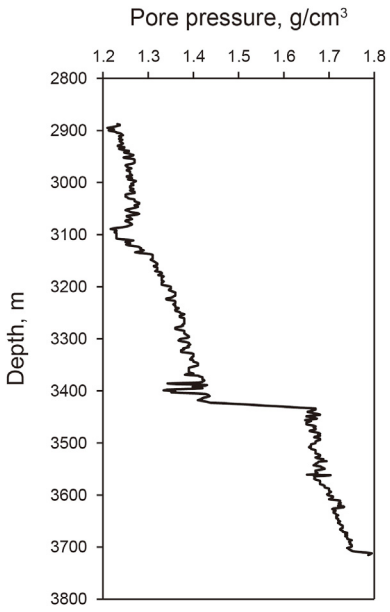


**Fig. 5.** Pore pressure of Well number 2.

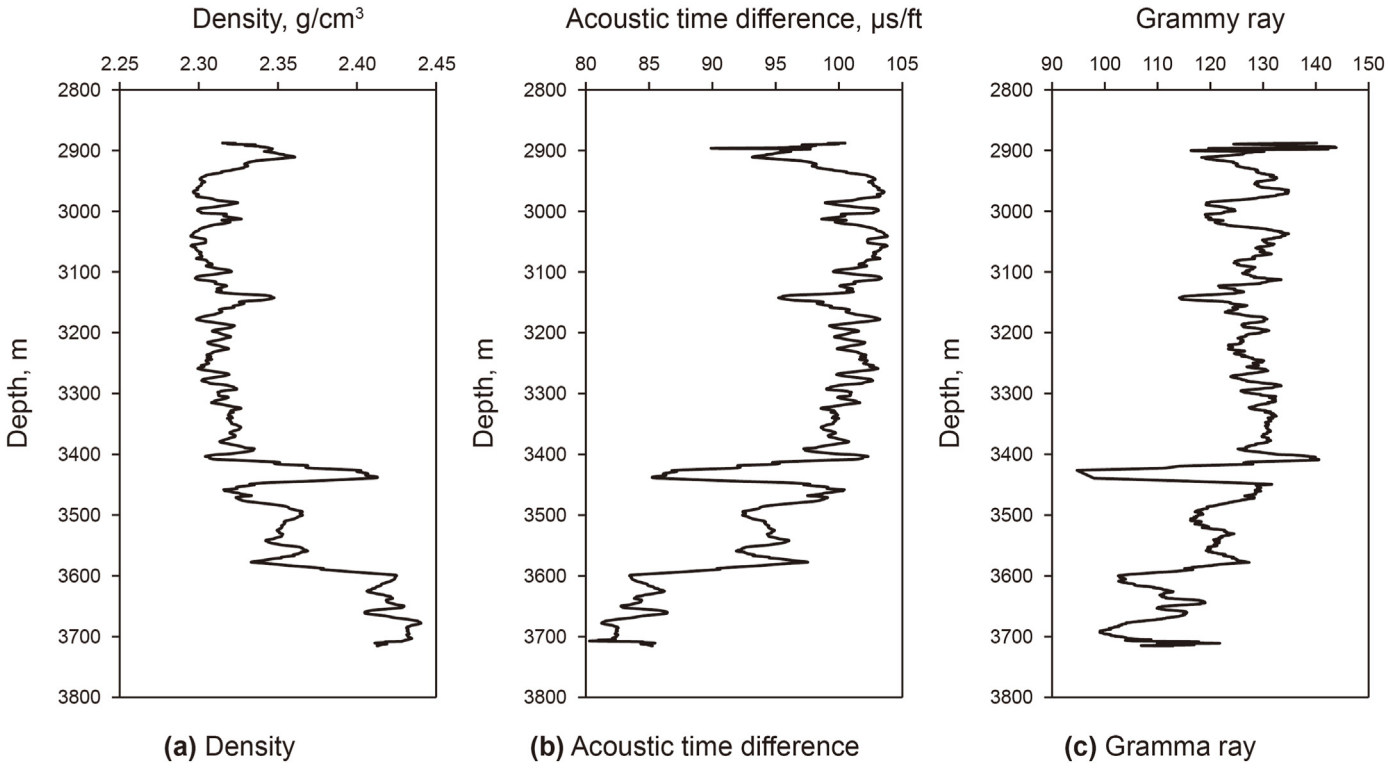


**Fig. 4.** Logging data of Well number 2.

$$Y = (\varphi_2(X) - \varphi_1(X))\eta + \varphi_1(X) \tag{7}$$

where, $Y$ is the Y coordinate of the point to be solved; $X$ is the X coordinate of the point to be solved; $\eta$ is the value obtained by random function.

By using a looping command to repeat the above operations multiple times, and the resulting ($X$, $Y$) will be the distribution coordinates of the virtual well.

Using the above method, the well location of the virtual well can be obtained as shown in the following Fig. 8.

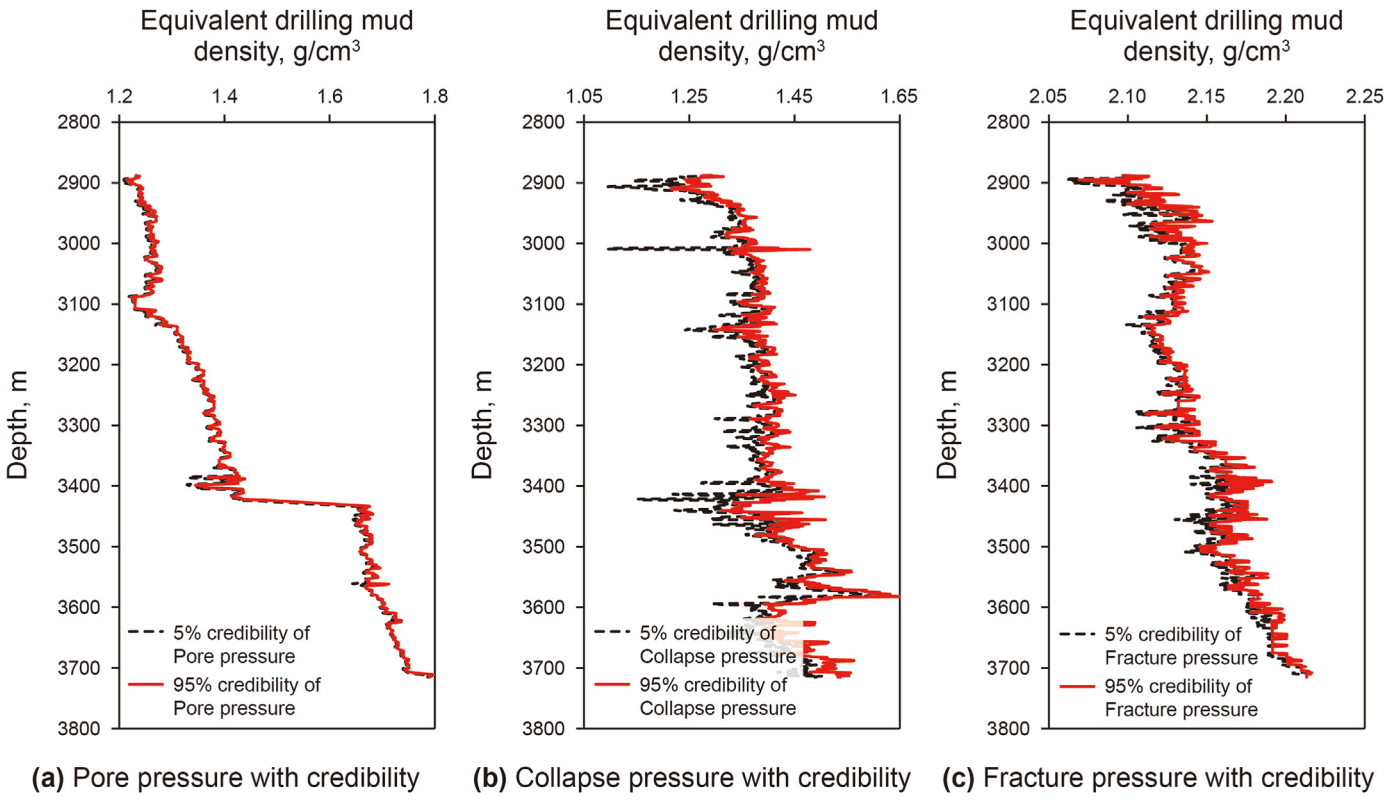


**Fig. 6.** Pressure with credibility of Well number 2.

### 3.2. Determination method of virtual well depth

According to the well history data, all eight drilled wells are vertical wells, and the virtual wells are also set as vertical wells. At the same time, in order to ensure that the data of the drilled wells can be fully considered when using the interpolation method to obtain the relevant properties of the virtual wells, the depth of the virtual wells is set to the bottom boundary of the deepest formation encountered by the eight drilled wells.

The bottom boundary of the deepest stratum that has been drilled in this block is T40. Based on this layer, the depths of eleven virtual wells in Fig. 8 are determined, as shown in the following Table 1.

### 3.3. Calculation method of seismic interval velocity for virtual well

The virtual well information involves a variety of data such as seismic interval velocity and rock mechanical parameters. Among them, the seismic interval velocity can be extracted from the 3D seismic interval velocity model. Based on the geodetic coordinates of the virtual well, the 3D seismic interval velocity model was established by combining the SEG-Y seismic body of the block (as shown in Fig. 9), and the single well seismic interval velocity of the virtual well was extracted from the model based on the borehole trajectory of the virtual well respectively.

The seismic interval velocities of the drilled and virtual wells are shown in Fig. 10.

### 3.4. Calculation method of rock mechanical parameters for virtual well

#### 3.4.1. Calculation method of rock mechanical parameters for drilled wells

Rock mechanical parameters mainly include static Poisson's ratio, static modulus of elasticity, internal friction angle, internal cohesion, uniaxial compressive strength and uniaxial tensile strength, which reflect the physical properties of the rocks under the action of external forces (Wu, 2020). They are also necessary parameter for calculating formation pressure. However, the acquisition of static mechanical parameters like static Poisson's ratio and static modulus of elasticity can be complex and costly (Li et al., 2020). Therefore, the method of dynamic and static conversion is often used in engineering, i.e., the dynamic mechanical parameters are first obtained by using logging data, and then the dynamic mechanical parameters are converted to static mechanical parameters by using the correction formula.

(1) Calculation of static Poisson's ratio and static modulus of elasticity

The conventional method is the triaxial experimental method, i.e., the static elastic model and Poisson's ratio are obtained by applying a constant surrounding pressure to the rock sample and gradually increasing stress in the axial direction until the sample is destroyed. However, this method is slow and costly, and it is

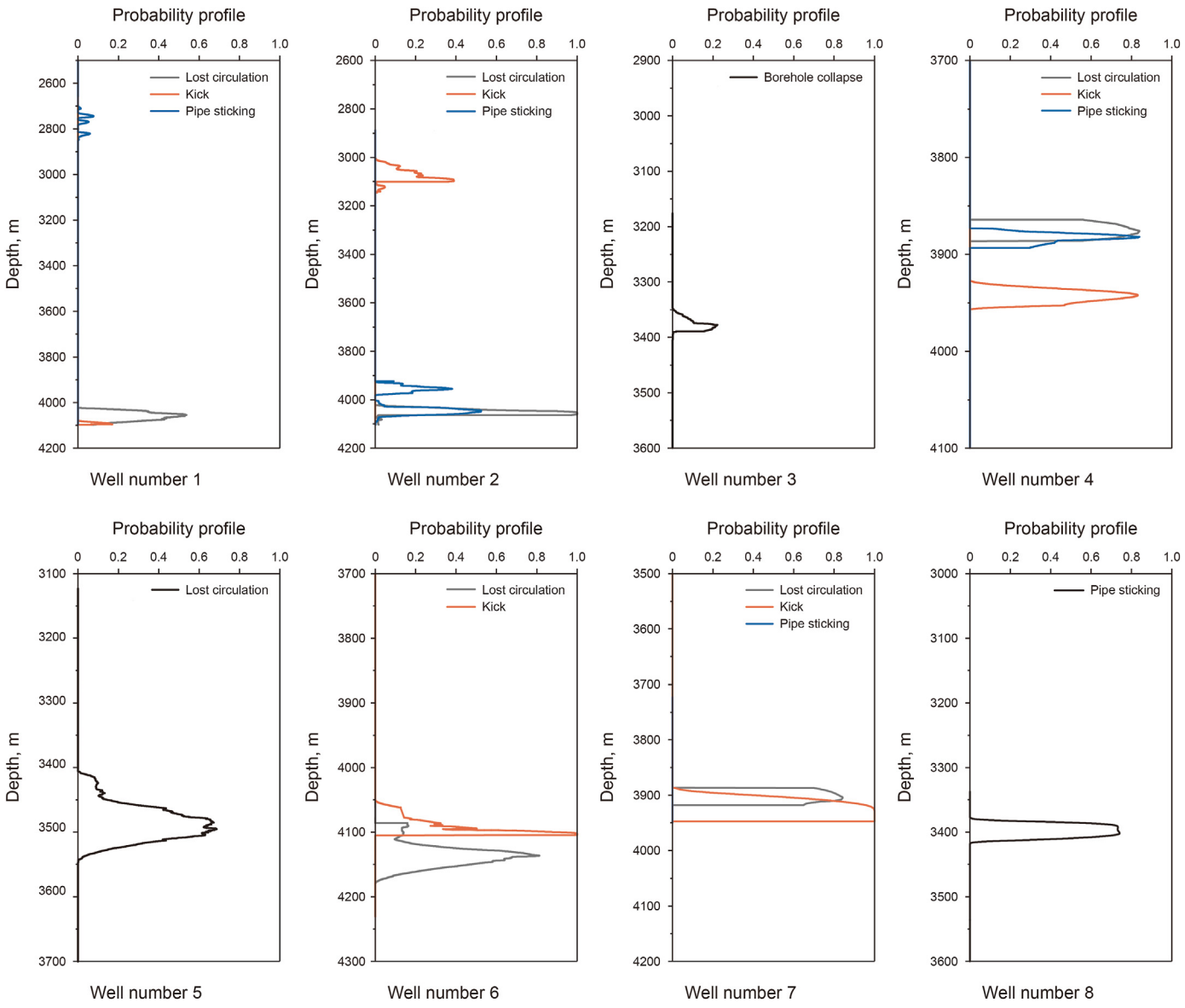


**Fig. 7.** Risk profiles of eight drilled wells.

difficult to obtain continuous data (Xu et al., 2014). Therefore, in practical applications, the conversion between dynamic and static is often achieved by linear regression method.

The calculation formulae of dynamic Poisson's ratio and dynamic modulus of elasticity are as follows:

$$\mu_d = \frac{V_p^2 - 2V_s^2}{2\left(V_p^2 - V_s^2\right)} \tag{8}$$

$$E_d = \frac{\rho V_s^2\left(3V_p^2 - 4V_s^2\right)}{V_p^2 - V_s^2} \times 10^3 \tag{9}$$

where, $\mu_d$: dynamic Poisson's ratio, nondimensional quantities; $E_d$: dynamic modulus of elasticity, $10^4$ MPa; $V_p$: P-wave velocities, km/s; $V_s$: S-wave velocities, km/s; $\rho$: rock density, g/cm$^3$.

The conversion formulae of static Poisson's ratio, static modulus of elasticity are as follows:

$$\mu_s = A_1 + K_1\mu_d \tag{10}$$

$$E_s = A_2 + K_2 E_d \tag{11}$$

where, $\mu_s$: static Poisson's ratio, nondimensional quantities; $A_1 = 0.1096$; $K_1 = 1.0385$; $\mu_d$: dynamic Poisson's ratio, nondimensional quantities; $E_s$: static modulus of elasticity, $10^4$ MPa; $A_2 = -0.082$; $K_2 = 0.74$; $E_d$: dynamic modulus of elasticity $10^4$ MPa.

(2) Calculation of uniaxial compressive strength and uniaxial tensile strength

Uniaxial compressive strength has different calculation formulae according to different lithologies. According to the well history data, we found that the block is mainly mudstone, so the calculation formulae of uniaxial compressive strength are as follows:

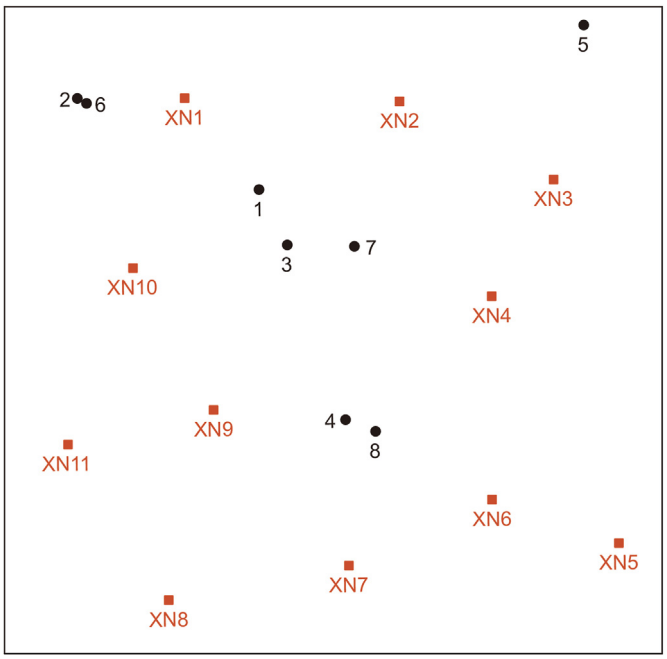


**Fig. 8.** Distribution of drilled wells and virtual wells in the block.

$$S_c = 0.033\rho^2 V_p^4 \left(\frac{1+\mu_d}{1-\mu_d}\right)^2 (1-2\mu_d)(1+0.78V_{sh}) \quad (12)$$

where, $S_c$: uniaxial compressive strength, MPa; $\rho$: rock density, g/cm$^3$; $V_p$: P-wave velocities, km/s; $\mu_d$: dynamic Poisson's ratio, nondimensional quantities; $V_{sh}$: mudstone content, nondimensional quantities.

The calculation formula of uniaxial tensile strength is as follows:

$$S_t = \frac{S_c}{K} \quad (13)$$

where, $S_t$: uniaxial tensile strength, MPa; $S_c$: uniaxial compressive strength, MPa; The value range of $K$ is 8~25, usually 12.

(3) Calculation of internal cohesion and internal friction angle

Internal cohesion can be calculated by rock density, acoustic velocity, mudstone content and dynamic Poisson's ratio. The calculation formula is as follows:

$$C = 0.00544\rho^2 V_p^4 \left(\frac{1+\mu_d}{1-\mu_d}\right)^2 (1-2\mu_d)(1+0.78V_{sh}) \quad (14)$$

where, $C$: internal cohesion, MPa; $\rho$: rock density, g/cm$^3$; $V_p$: P-wave velocities, km/s; $\mu_d$: dynamic Poisson's ratio, nondimensional quantities; $V_{sh}$: mudstone content, nondimensional quantities.

The calculation formula of internal friction angle is as follows:

$$\varphi = a \cdot \log\left[M + \left(M^2+1\right)^{\frac{1}{2}}\right] + b \quad (15)$$

$$M = a_1 - b_1 C \quad (16)$$

where, $\varphi$: internal friction angle, °; $a = 2.654$; $b = 20$; $a_1 = 58.93$; $b_1 = 1.785$; $C$: internal cohesion, MPa.

Using Eqs. (8)–(16) to calculate the rock mechanical parameters of eight drilled wells, the final rock mechanical parameters are shown in Fig. 11.

### 3.4.2. Calculation method of rock mechanical parameters for virtual wells

For the prediction of rock mechanical parameters of virtual wells, we propose two methods: the prediction method based on deep learning and well seismic data fusion, and the prediction method based on the combination of Ordinary Kriging Interpolation and Depth Adjustment. In Appendix II, we provide a detailed analysis of the applicability and accuracy of the two methods. The results show that the prediction accuracy of both methods is poor when the number of drilled wells in the area is small and unevenly distributed. If the drilling wells are relatively evenly distributed, the prediction results of the second method can be used as a reference. When the number of drilled wells in the area is appropriate (the case in this paper), the prediction accuracy of the two methods is not much different, so the second method is used in this paper, and the prediction results are shown in Fig. 12.

## 4. Regional drilling risk prediction method based on deep learning

The seismic interval velocity as well as rock mechanical parameters of the virtual wells obtained in the previous section provide rich data support for the next deep learning. The steps of regional drilling risk prediction using deep learning are as follows: First, an intelligent model based on deep learning is used to quantitatively evaluate the correlation between the rock mechanical parameters of the drilled wells, the seismic interval velocity and the downhole risk. Second, the obtained correlation is used to predict the risk of the virtual well by combining the rock mechanical parameters and seismic interval velocity of the virtual well. The detailed process is shown in Fig. 13.

### 4.1. Optimization of intelligent model

Currently, the commonly used intelligent models for risk prediction include BP neural network (Shaik et al., 2020), Bayesian network (Liu et al., 2021; Zinke et al., 2020), Logistic regression, RNN model and LSTM model. In order to select the optimal model, seven drilled wells (Well number 1, Well number 2, Well number 3, Well number 5, Well number 6, Well number 7 and Well number 8) were used as the training set, while the risk profile data of Well number 4 was used as the test set. The risk prediction values of the Well number 4 obtained from seven drilled wells were compared with the actual value (original risk data). By drawing the confusion matrix (Ahmad et al., 2022; Theissler et al., 2022; Wang et al., 2022) of risk prediction results, the performance of each commonly used

**Table 1**
Depth of virtual wells.

| Name | XN1 | XN2 | XN3 | XN4 | XN5 | XN6 | XN7 | XN8 | XN9 | XN10 | XN11 |
|---|---|---|---|---|---|---|---|---|---|---|---|
| Depth, m | 3942.59 | 3890.62 | 3953.33 | 3920.19 | 4360.61 | 4251.6 | 4382.36 | 4441.11 | 4279.54 | 4266.8 | 4471.5 |

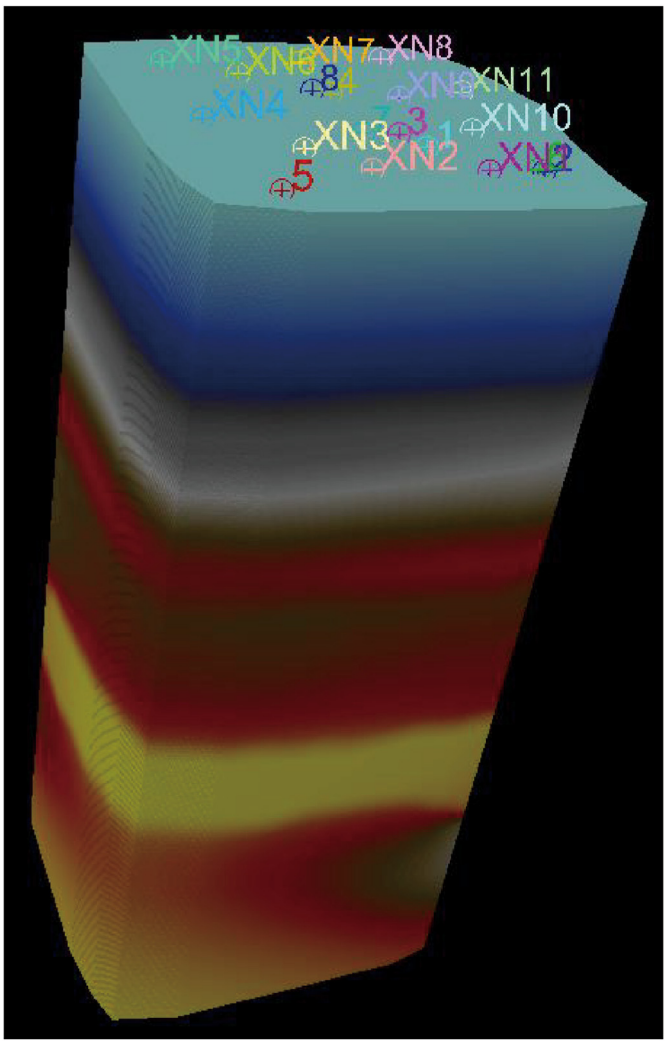


**Fig. 9.** 3D seismic interval velocity model.

intelligent model was evaluated, as shown in Fig. 14. It can be seen that the LSTM model has a high accuracy in predicting lost circulation, kick, borehole collapse and pipe sticking in different downhole complexities. Therefore, the LSTM model was selected to analyze and predict risks.

### 4.2. Structure of LSTM

The LSTM (Long Short Term Memory) model is a variant of the RNN model, and the most important feature of this kind of model is that the neurons can be fed again as inputs after being output at some point (Song et al., 2022), which can maintain the dependencies in the data. Compared with the traditional neural network, it can process the data of sequence change (Pan et al., 2021). The key of the LSTM is the cell state, the horizontal line running through it above. The cell state is similar to a conveyor belt that runs directly over the entire chain with only some few linear interactions, which ensures that information is transmitted over it without loss. In addition, the LSTM is elaborated with structures called "gates" to remove or increase information into the cell state, including forget gate, input gate and output gate (Cheng et al., 2019). The structure of the LSTM model is shown in Fig. 15

Firstly, the forget gate determines what information we discard from the cell state:

$$f_t = \sigma\left(W_f[h_{t-1}, x_t] + b_f\right) \tag{17}$$

Then, the input gate calculates what part of the input data can be stored into the cell state:

$$i_t = \sigma(W_i[h_{t-1}, x_t] + b_i) \tag{18}$$

$$\tilde{C}_t = \tanh(W_c[h_{t-1}, x_t] + b_c) \tag{19}$$

Next, the old cell state $C_{t-1}$ from the previous state is updated to the current state $C_t$:

$$C_t = f_t * C_{t-1} + i_t * \tilde{C}_t \tag{20}$$

Finally, the output gate needs to determine what value to output, and this output will be based on our cell state:

$$o_t = \sigma(W_o[h_{t-1}, x_t] + b_o) \tag{21}$$

$$h_t = o_t * \tanh(C_t) \tag{22}$$

where, $W_f$, $W_i$, $W_c$, $W_o$ are the hidden layer weight values between the current hidden layer and the previous hidden layer, and $b_f$, $b_i$, $b_c$, $b_o$ are the deviation vectors (Lin et al., 2022). $\sigma$ and tanh are the activation functions. The formula of $\sigma$ is Eq. (23), which can convert all the calculated data to the (0, 1).

$$S(x) = \frac{e^x}{e^x + 1} \tag{23}$$

The calculation formula of the activation function tanh is Eq. (24), which can convert the calculated data to (−1, 1).

$$f(x) = \frac{e^x - e^{-x}}{e^x + e^{-x}} \tag{24}$$

### 4.3. Construction method of LSTM input model

The first step in LSTM model prediction is to train the model to find correlations between input and output attributes. In this paper, the input $x_t$ of the training model is the rock mechanical parameters of the drilled wells calculated by logging data (including static Poisson's ratio, static elastic of modulus, internal friction angle, internal cohesion, uniaxial compressive strength and uniaxial tensile strength), with seismic interval velocity, and each attribute corresponds to depth one by one. The output $h_t$ is the corresponding risk (lost circulation, kick, borehole collapse and pipe sticking). As shown in Fig. 16.

From the risk profile of drilled wells, it is evident that the length of the risk-section of a well is particularly short, with the majority of sections having a risk probability data of "0". However, when there are too much "0" data, it inevitably affects the quality of training. Therefore, in order to reduce computation and shorten the training time, it is necessary to remove some of the "0" data, so that the final non-"0" risk data segments account for about 90%–95% of the total data. In addition, the data must be deleted from both ends of the data set to ensure that the training part of the depth data is continuous and the step size is consistent. In this paper, the step size of the training and prediction sets is 0.1 m. If a well contains multiple risk scenarios, each risk should be predicted separately.

In addition, there may be anomalous data in the data caused by a variety of unknown factors, which may produce biased prediction results for the model (Boulmaiz et al., 2020). In order to minimize the influence of unknown factors, the data set is input and then

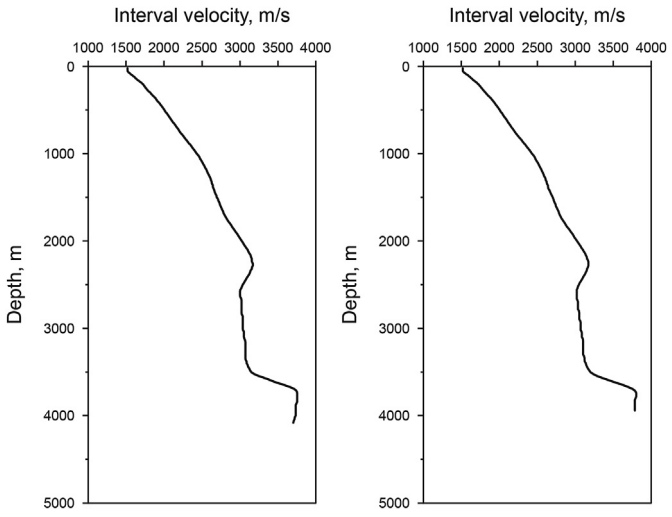


**(a)** The seismic interval velocity of drilled wells (Take Well number 1 as an example, the remaining figure are in Appendix III)

**(b)** The seismic interval velocity of virtual wells (Take XN1 as an example, the remaining figure are in Appendix III)

**Fig. 10.** The seismic interval velocity of drilled wells and virtual wells.

randomly sorted before dividing the data set, and the first 90% of the new data set formed after sorting is used as the training segment and the last 10% as the validation segment, as shown in Fig. 17.

In Fig. 17, $h_0$ and $C_0$ are the initial states of the hidden layer of the LSTM neural network, while $h_{d-1}$ and $C_{d-1}$ are the outputs of the 90% training section, which are passed at the beginning of 10% validation section as input. Assuming that the sample point number at the beginning of the validation section is $d$, then based on $h_{d-1}$ and $C_{d-1}$ calculated at $d-1$, combined with rock mechanical parameters and interval velocity at $d$, $h_d$ and $C_d$ at $d$ are predicted, and then the risk at $d$ can be calculated. Next, according to $h_d$ and $C_d$ at $d$, together with the rock mechanical parameters and interval velocity at $d$, $h_{d+1}$ and $C_{d+1}$ and risk at $d+1$ are calculated (Zhang et al., 2018). The cycle is repeated to finalize the training and validation of the model.

When building a risk prediction model, in addition to dividing the data set, it is necessary to standardize the data, which can avoid the influence of dimension on the model learning, thereby significantly improve the training speed of the model (Zhou et al., 2021). The input feature contains seven dimensions, and the output feature includes one dimension. Consequently, the number of cell units in the input layer is set to seven, and the number of cell units in the output layer is one, while the number of cell units in the hidden layer is determined according to the empirical formula (Wei et al., 2013a, b). In order to accelerate the learning speed of the network, the Adam optimization algorithm was used, and 500 rounds of training were performed. Besides, the gradient threshold was also set to 1 to prevent gradient explosion, and the initial learning rate of 0.001 was specified and reduced after 20 rounds of training by multiplying by a factor of 0.9. Finally, the LSTM prediction results are back-normalized to obtain the corresponding risk data. The entire prediction structure is shown in Fig. 18, where the computation of the hidden layer is the core of the network (Wang et al., 2020).

### 4.4. Construction method of LSTM prediction model

The prediction model utilizes the correlation of the training model to predict the risk of virtual wells. The prediction model data set is processed in the same way as the training model. Considering the continuity of layer, the sedimentary structure of adjacent wells is identical (Zhang et al., 2012). Consequently, when predicting virtual wells, in order to make the prediction results more reliable and strengthen the correlation between the data, the "close interval prediction method" was proposed. According to the depth interval of the drilling risk data, the prediction depth interval of the virtual well is selected similarly, e.g., if the depth interval of a certain risk data is 2500–2550 m, the depth interval of the virtual well can be selected as 2450–2600 m.

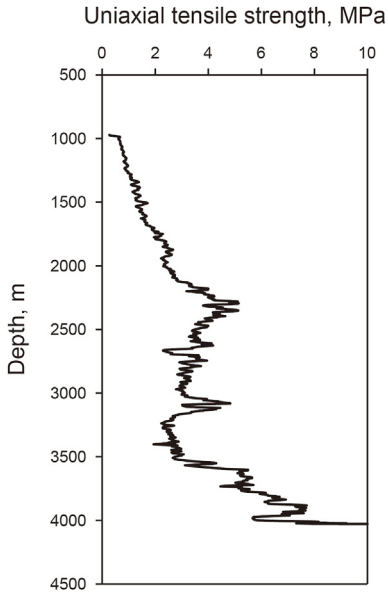


**Fig. 11.** Rock mechanical parameters of drilled wells. (take uniaxial tensile strength of Well number 1 as an example, the remaining figure are in Appendix III).

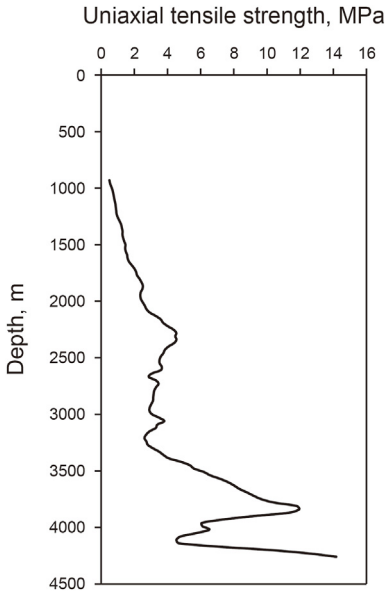


**Fig. 12.** Rock mechanical parameters of drilled wells. (take uniaxial tensile strength of Well number 1 as an example, the remaining figure are in Appendix III).

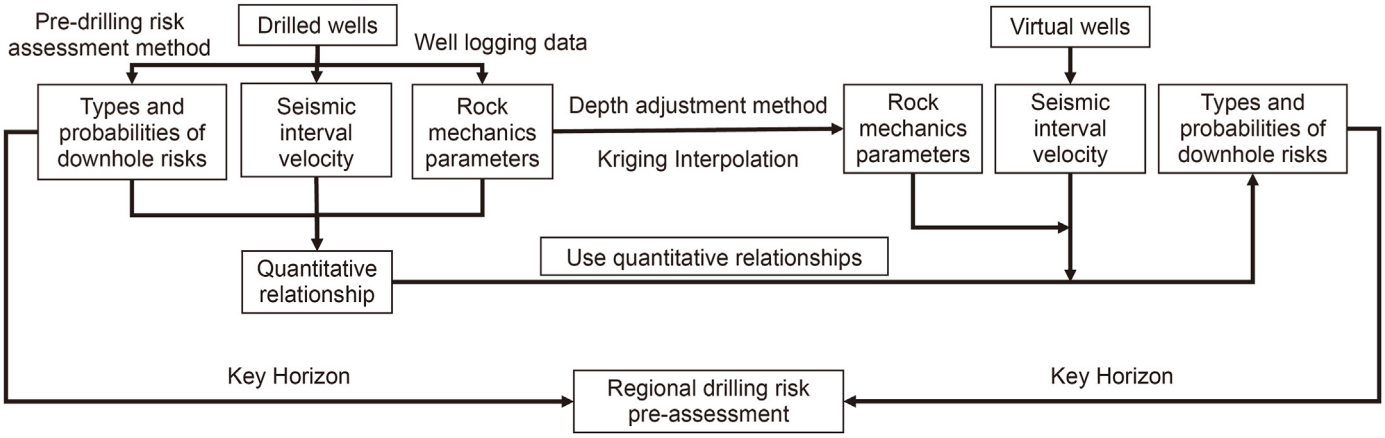


**Fig. 13.** Basic process of regional drilling risk pre-assessment.

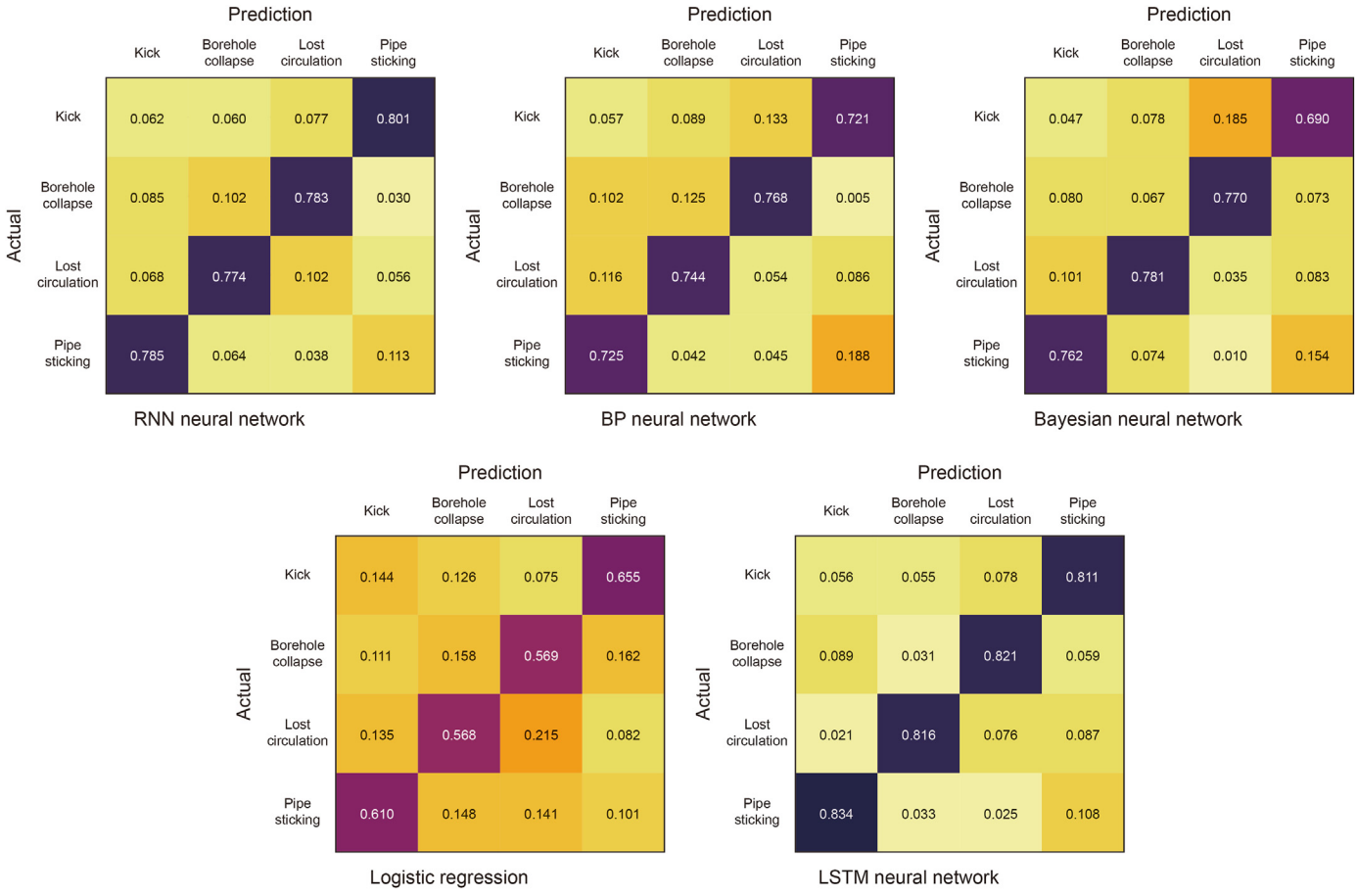


**Fig. 14.** Confusion matrix of risk prediction results of commonly used intelligent models.

### 4.5. Prediction effect analysis

Seven drilled wells (Well number 1, Well number 2, Well number 3, Well number 5, Well number 6, Well number 7 and Well number 8) were used as the training set, and the Well number 4 was used as the test set to analyze the prediction accuracy of the constructed LSTM model. The training results of the seven drilled wells were as shown in Fig. 19.

It can be seen that the test data profiles of the LSTM for the four risks and the actual data profiles not only have similar trends but also have similar values, which proves that the predictions of the LSTM for the 10% training data segment have a high degree of confidence. Using the quantitative relationships obtained for the Well number 4, the predicted risk profiles of the Well number 4 is compared with the actual risk profiles as shown in Fig. 20.

The same method was used to verify Well number 1, the predicted results are shown in Fig. 21.

It can be seen from Figs. 20 and 21 that the prediction of the

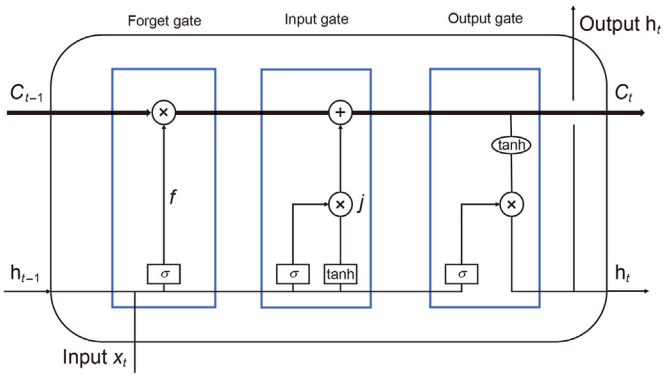


**Fig. 15.** The structure of the LSTM.

occurrence depth and probability of each risk were basically consistent with the actual risk profile and the actual risks situation.

In addition, there is no risks case of borehole collapse in the well history of Well number 4, and the predicted risk of borehole collapse was less than 0.2, which was consistent with the actual situation. Using the actual and predicted risk profile maximums as the standard, the prediction error was calculated and the relative error of the model was 9.19%.

### 4.6. Virtual well risk profile prediction

Using the trained model to foresee the risk of virtual wells, the risk profile of the virtual wells are as shown in Fig. 22.

## 5. Construction method of regional 3D risk body

In order to analyze the impact of adding virtual wells on the block risk prediction accuracy, one of the eight drilled wells is selected as the control well. Based on the sequential Gaussian simulation method, the block risk model was constructed with the

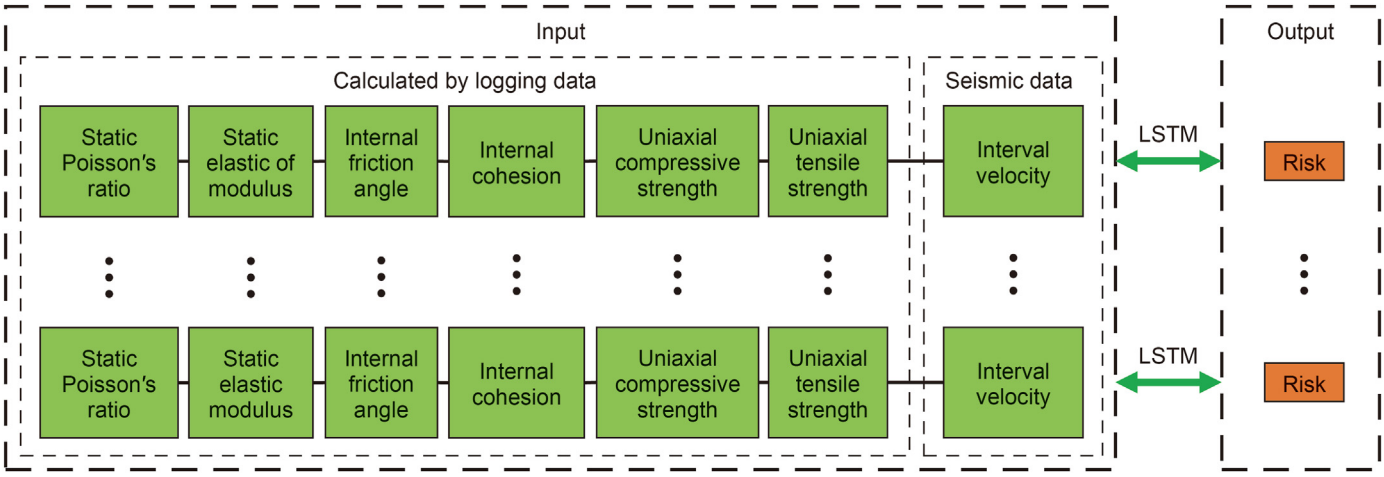


**Fig. 16.** Diagram of the input and output of the model.

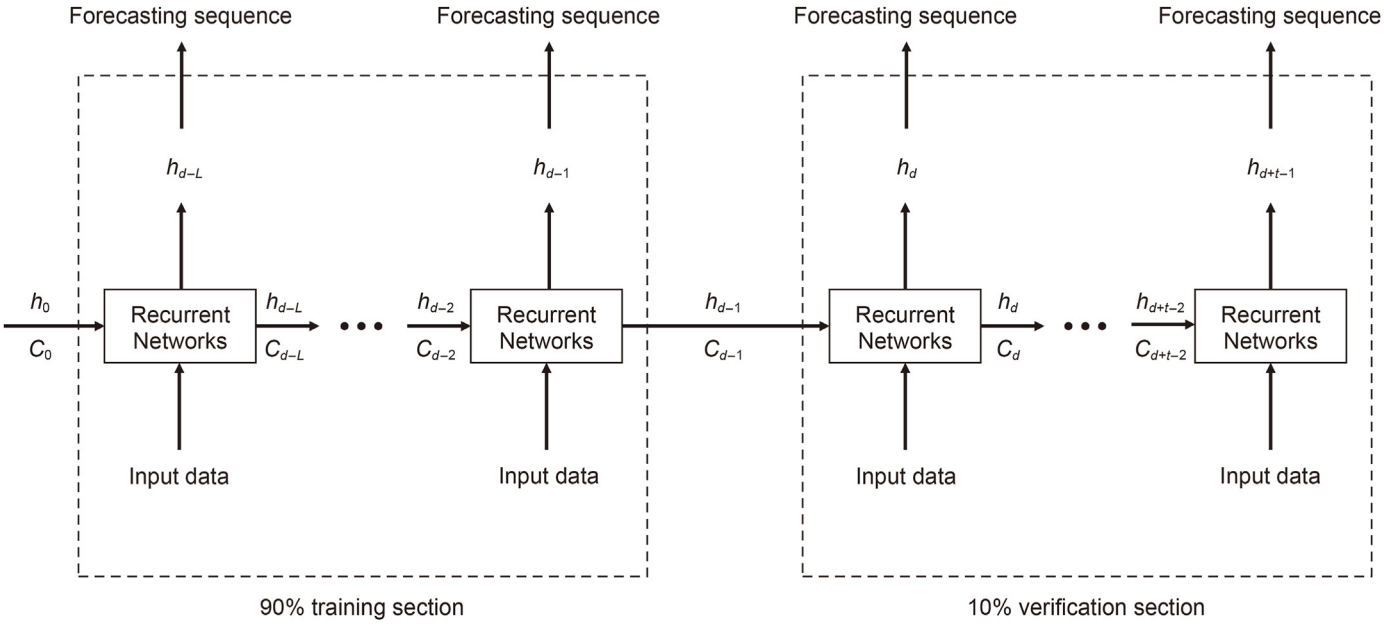


**Fig. 17.** Training process.

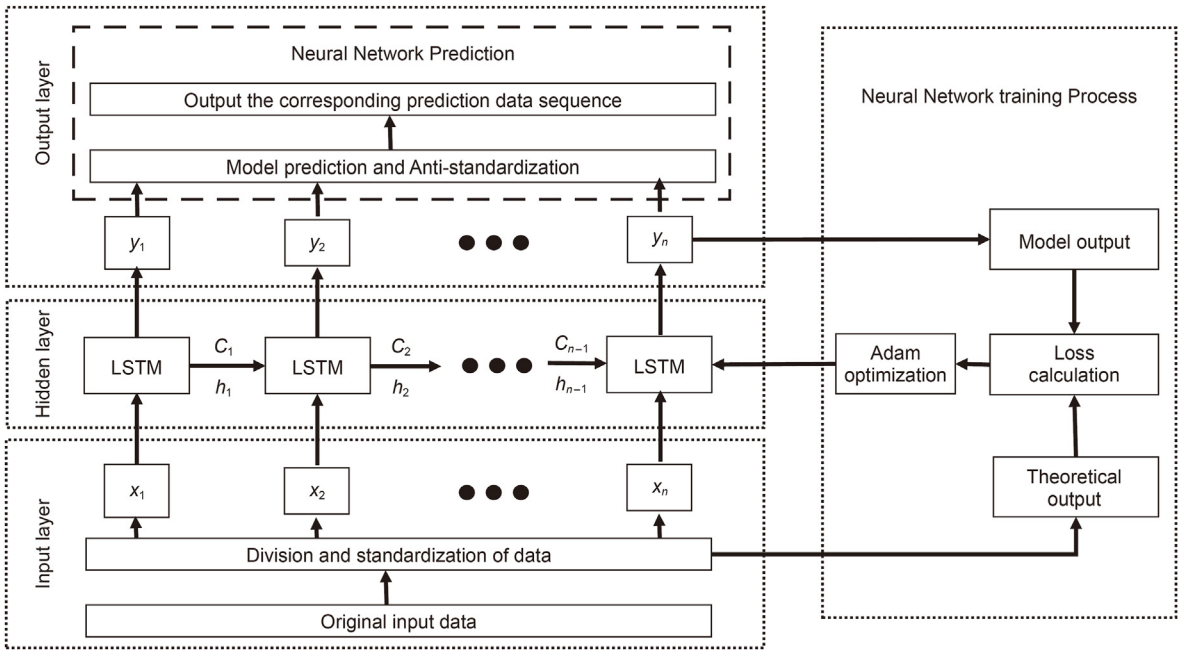


**Fig. 18.** LSTM network prediction framework.

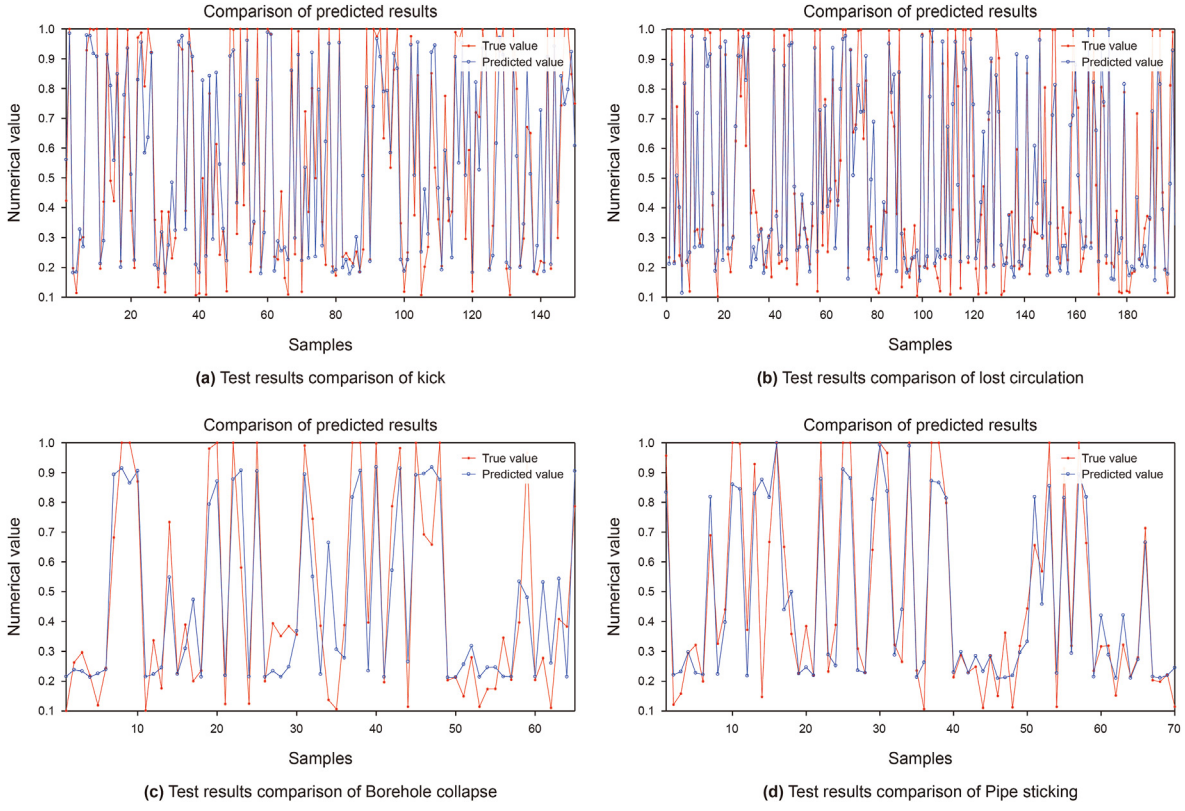


**(a)** Test results comparison of kick

**(b)** Test results comparison of lost circulation

**(c)** Test results comparison of Borehole collapse

**(d)** Test results comparison of Pipe sticking

**Fig. 19.** Comparison of risk test results.

remaining seven drilled wells and the block risk model after adding eleven virtual wells was built by using the geological modeling software. The risk data of the control well are extracted from the two models and compared with the actual risk occurrence locations obtained from the well history data to determine the impact of the virtual wells on the risk prediction accuracy.

### 5.1. Sequential Gaussian simulation method

Sequential Gaussian simulation is a stochastic simulation

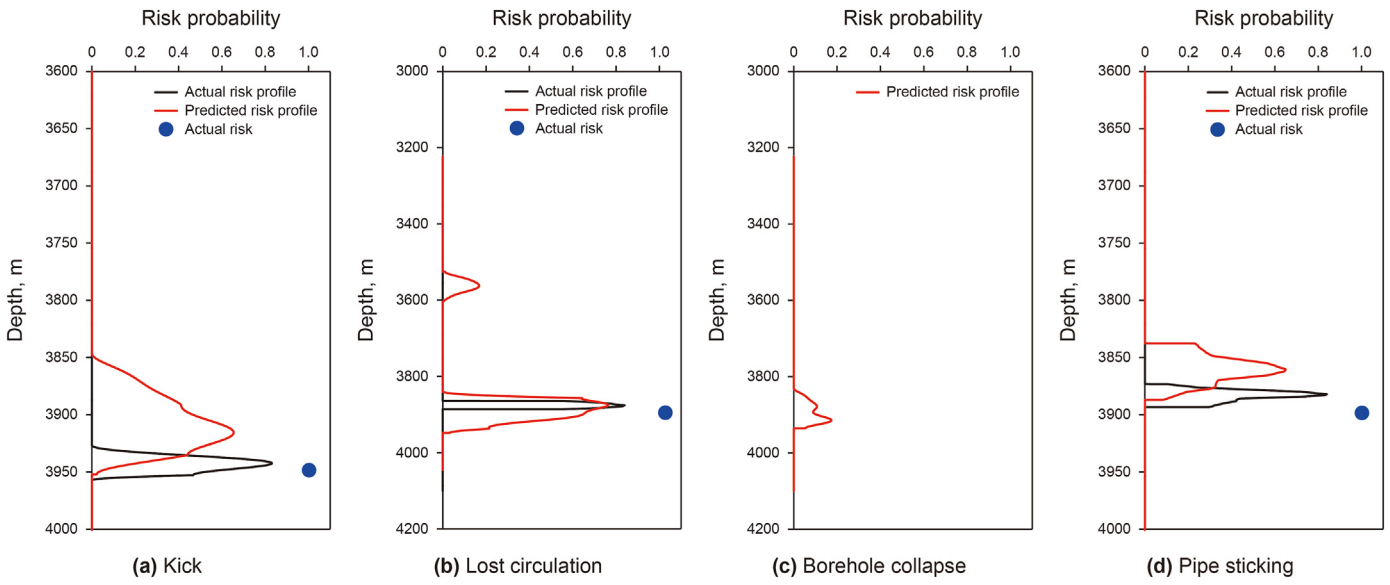


**Fig. 20.** Well number 4 risk comparison.

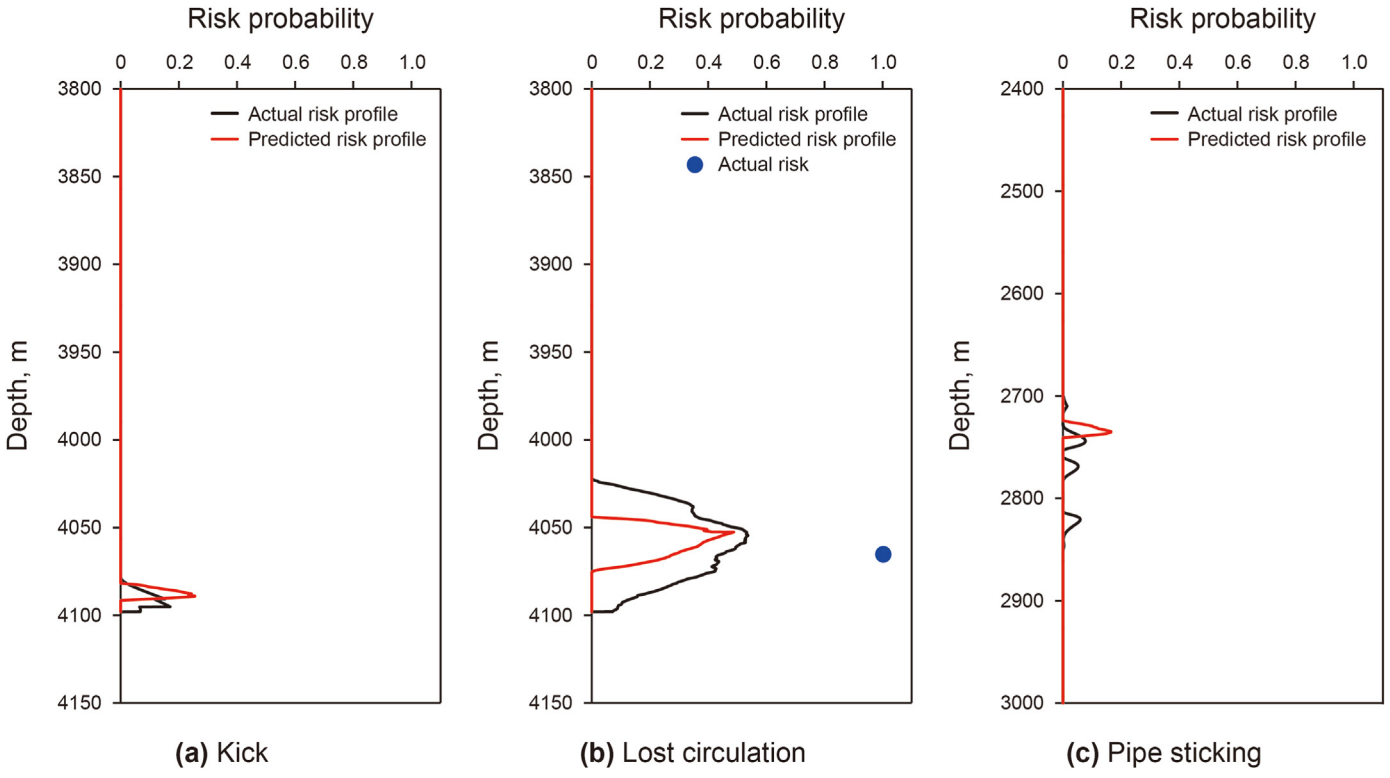


**Fig. 21.** Risk comparison of Well number 1.

method that applies Gaussian probability theory and sequential simulation algorithm to generate the spatial distribution of continuous variables (Wang et al., 2012; Bai and Tahmasebi, 2022). It is one of the most widely used stochastic modeling method for continuous geological variables, and the basic idea is to perform sequential simulation of conditional data obeying normal distribution (Gao, 2014). The Gaussian function is constructed according to the known data, and each value of the regionalized random variable $Z(x)$ is regarded as a random realization conforming to the Gaussian function $F(x)$. At each simulated location $x_m$, $F(x)$ is a cumulative conditional probability density function with the $n$ known data $Z(x_j)(j=0,1,2,\cdots,n)$ and the $m-1$ simulated values $Z(x_i)(i=1,2,\cdots,m-1)$ (Zhao et al., 2011).

### 5.2. Comparative analysis

From the eight drilled wells, Well number 4 was selected as the control well. Based on the risk data of the remaining seven wells,

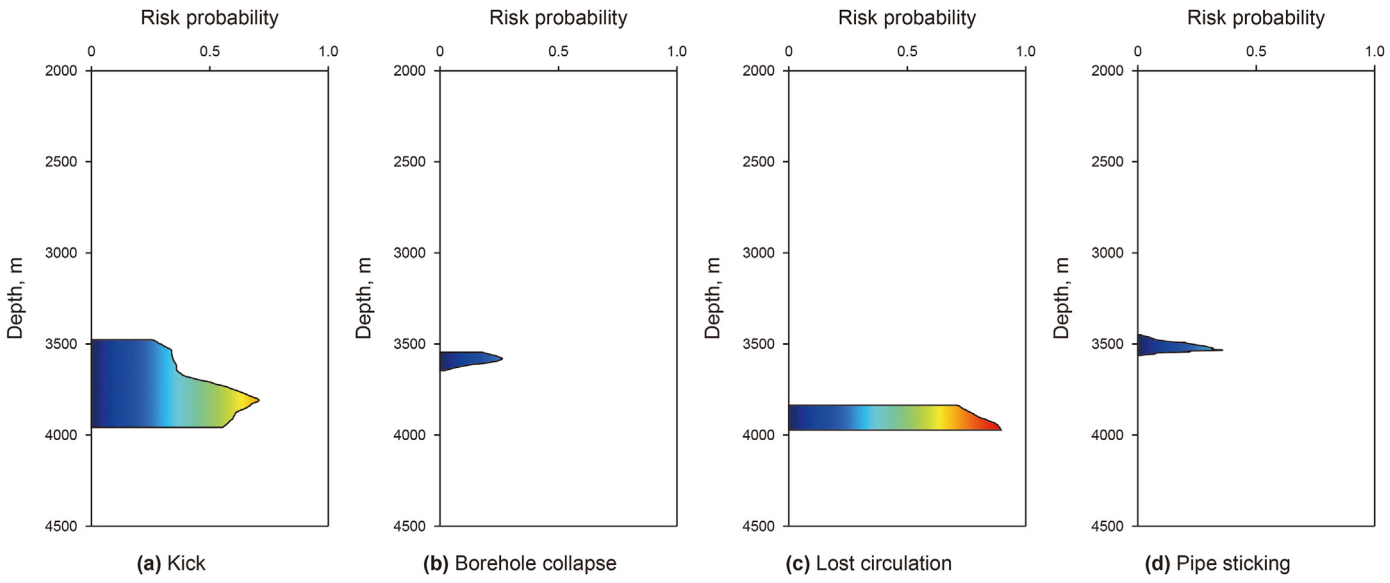


**Fig. 22.** Risk profile of virtual wells. (take XN1 as an example, the remaining figure are in Appendix III).

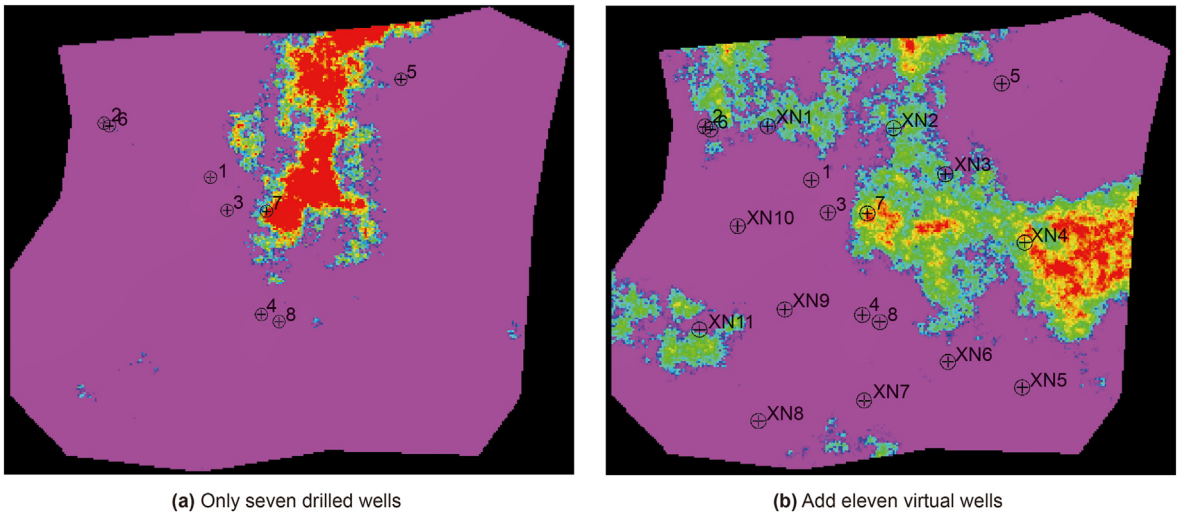


**Fig. 23.** Kick risk model at T30 level.

according to the sequential Gauss simulation method in combination with the seismic interpretation layer, a three-dimensional risk model of the block with only seven drilled wells was established layer by layer, and the risk data of Well number 4 were extracted from the three-dimensional risk model. Then, on the basis of seven drilled wells, the risk data of eleven virtual wells were added, and the 3D risk model of the block was also established according to the hierarchical group of sequential Gaussian simulation method, from which the risk data of Well number 4 were extracted. The risk data of Well number 4 extracted twice were compared with the actual risk location of Well number 4 based on the well history data, and the results are shown in Fig. 24.

It can be seen from Fig. 23 that the 3D risk model after adding eleven virtual wells is significantly richer in color, i.e., the risk information was richer than the model established with only seven drilled wells. From Fig. 24, it can also be seen that the location interval of the risk occurrence of Well number 4 extracted with only seven drilled wells for the first time is obviously far from the location of the actual risk occurrence, while the risk interval of Well number 4 after adding eleven virtual wells for the second time is not much different from the location of the actual risk. The accuracy was calculated using the maximum value of the risk profiles extracted from both times, and the highest prediction accuracy was improved by 21% in the second time.

The same method is used to verify Well number 5, the result is shown in Fig. 25.

Similarly, the risk profile data extracted after adding virtual wells in Fig. 25 is more accurate than the data extracted using only the drilled wells. This shows that the risk model built by relying only on the risk data of drilled wells cannot make accurate risk prediction for the whole block, while the risk model built after adding eleven virtual wells can significantly improve the fineness of regional risk prediction, which verifies the feasibility of the method.

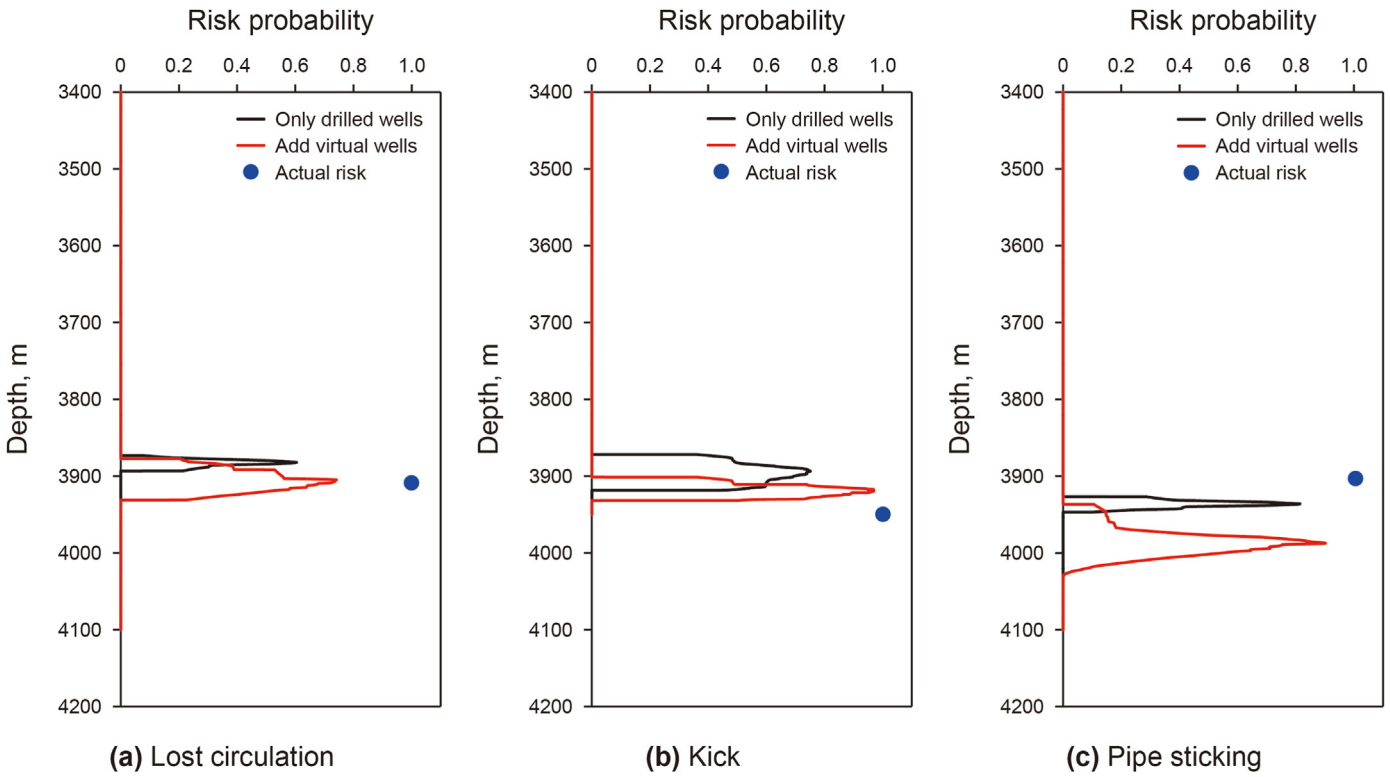


**Fig. 24.** Risk comparison of Well number 4.

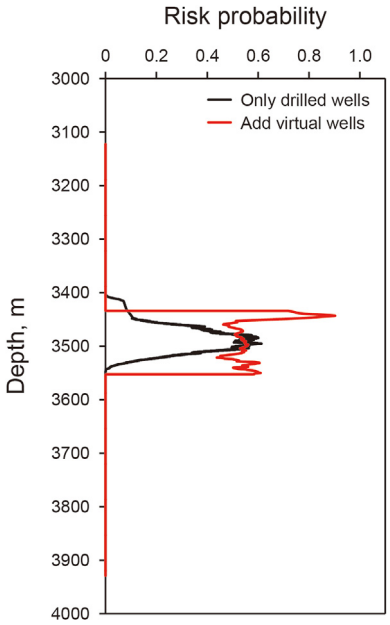


**Fig. 25.** Risk comparison of Well number 5.

## 6. Conclusion

(1) Based on the risk profiles calculated by the pre-drill risk evaluation method, it contains rich geological and engineering information. Using them as sample data for the training of the intelligent model not only solves the problem of small number of risk samples, but also incorporates physical knowledge (wellbore pressure balance criterion) constraints for the training set, which improves the model reliability.

(2) The prediction method of virtual wells and their related parameters proposed in this paper can better solve the problem of small number and uneven distribution of drilled wells in new exploration areas. Using the preferred LSTM model, the quantitative relationship between the seismic, logging, rock mechanical parameters, other multi-source data of drilled wells and the drilling risk profile is explored, and the drilling risk profile of virtual wells is predicted. Finally, the drilling risk profile with uniform distribution of well locations in the area is obtained, which significantly improves the accuracy of the pre-drilling three-dimensional risk predictor. Compared with not adding virtual wells, the accuracy of risk prediction in unexplored areas has been improved by 21% at most.

(3) Reliable data set is the basis of intelligent model training and guarantee the accuracy of prediction results. Since the drilling risk in the study area is basically caused by pressure imbalance, the calculation method of drilling risk profile based on wellbore pressure balance is applicable. However, for the more complex drilling risks that are not caused by pressure imbalance, it is recommended to further investigate the correction method of risk profiles of drilled wells, so that the drilling risk sample data can be maximized to match the actual situation and incorporate more physical knowledge.

## Fund project

General Program of National Natural Science Foundation of China (52274024, 52074326)

## Declaration of competing interest

No potential conflict of interest was reported by the authors.

## Appendix A. Supplementary data

Supplementary data to this article can be found online at https://doi.org/10.1016/j.petsci.2023.06.005.

## References

Abimbola, M., Khan, F., 2016. Development of an integrated tool for risk analysis of drilling operations. Process Saf. Environ. Protect. 102, 421–430. https://doi.org/10.1016/j.psep.2016.04.012.

Abimbola, M., Khan, F., 2018. Dynamic blowout risk analysis using loss functions. Risk Anal. 38 (2), 255–271. https://doi.org/10.1111/risa.12879.

Adedigba, S.A., Oloruntobi, O., Khan, F., et al., 2018. Data-driven dynamic risk analysis of offshore drilling operations. J. Petrol. Sci. Eng. 165, 444–452. https://doi.org/10.1016/j.petrol.2018.02.049.

Ahmad, S., Ansari, S.U., Haider, U., et al., 2022. Confusion matrix-based modularity induction into pretrained CNN. Multimed. Tool. Appl. 81 (16), 23311–23337.

Alkinani, H.H., Al-Hameedi, A.T.T., Dunn-Norman, S., 2020. Artificial neural network models to predict lost circulation in natural and induced fractures. SN Appl. Sci. 2 (12), 1–13. https://doi.org/10.1007/S42452-020-03827-3.

Alkinani, H.H., Al-Hameedi, A.T.T., Dunn-Norman, S., 2021. Minimizing Lost Circulation Non-productive Time Using Expected Monetary Value and Decision Tree Analysis. SPE Western Regional Meeting, OnePetro.

Bai, T., Tahmasebi, P., 2022. Sequential Gaussian simulation for geosystems modeling: a machine learning approach. Geosci. Front. 13 (1), 7–20. https://doi.org/10.1016/J.GSF.2021.101258.

Boulmaiz, T., Guermoui, M., Boutaghane, H., 2020. Impact of training data size on the LSTM performances for rainfall–runoff modeling. Model. Earth Syst. Environ. 6, 2153–2164. https://doi.org/10.1007/s40808-020-00830-w.

Cheng, Y., Kang, Q., Wang, C., et al., 2019. Sentiment analysis of movie review based on LSTM. In: Proceedings of Proceedings of 2019 the 9th International Workshop on Computer Science and Engineering, pp. 275–282. https://doi.org/10.26914/c.cnkihy.2019.038215.

Gao, Y., 2014. Study on Geological Modeling Method of Oil and Gas Reservoir. Ph. D. Dissertation,. Xi'an University of Science and Technology (in Chinese).

Guan, Z.C., Ke, K., Lu, B.P., 2009. An approach to casing program design with formation pressure uncertainties. J. China Univ. Petrol. (Ed. Nat. Sci.) 33 (4), 71–75. https://doi.org/10.3321/j.issn:1673-5005.2009.04.013 (in Chinese).

Guan, Z.C., Wei, K., Fu, S.L., et al., 2013. Risk evaluation method for drilling engineering based on interval analysis. Petrol. Dril. Techniq. 41 (4), 15–18. https://doi.org/10.3969/j.issn.1001-0890.2013.04.004 (in Chinese).

He, C., Wang, Z.M., 2010. High sour gas well risk assessment based on analytic Hierarchy process. Drill. Prod. Technol. 33 (2), 28–30+37+137. https://doi.org/10.3969/j.issn.1006-768X.2010.02.009 (in Chinese).

Islam, R., Khan, F., Venkatesan, R., 2017. Real time risk analysis of kick detection: testing and validation. Reliab. Eng. Syst. Saf. 161, 25–37. https://doi.org/10.1016/j.ress.2016.12.014.

Jahanbakhshi, R., Keshavarzi, R., Jalili, S., 2014. Artificial neural network-based prediction and geomechanical analysis of lost circulation in naturally fractured reservoirs: a case study. Eur. J. Environ. Civ. Eng. 18 (3), 320–335. https://doi.org/10.1080/19648189.2013.860924.

Ke, K., 2019. Casing Level and Depth in Deepwater Drilling. Ph. D. Dissertation,. China University of Petroleum (East China) (in Chinese).

Ke, K., Guan, Z.C., Zhou, H., 2009. An approach to determining pre-drilling formation pore pressure with credibility for deep water exploration wells. J. China Univ. Petrol. (Ed. Nat. Sci.) 33 (5), 61–67. https://doi.org/10.3321/j.issn:1673-5005.2009.05.012 (in Chinese).

Li, J., Li, X.R., Zhan, H.B., et al., 2020. Modified method for fracability evaluation of tight sandstones based on interval transit time. Petrol. Sci. 17 (2), 477–486. https://doi.org/10.1007/s12182-019-00397-x.

Li, Z., Chen, M., Jin, Y., et al., 2018. Study on intelligent prediction for risk level of lost circulation while drilling based on machine learning. In: 52nd US Rock Mechanics/Geomechanics Symposium. OnePetro.

Liang, H., Zou, J., Li, Z., et al., 2019. Dynamic evaluation of drilling leakage risk based on fuzzy theory and PSO-SVR algorithm. Future Generat. Comput. Syst. 95, 454–466. https://doi.org/10.1016/j.future.2018.12.068.

Lin, R.G., Wang, H.W., Che, C.C., et al., 2022. Predictive maintenance model of aeroengine based on LSTM classifier. J. Syst. Eng. Electron. 44 (3), 1052–1059. https://doi.org/10.12305/j.issn.1001-506X.2022.03.39 (in Chinese).

Liu, B.Z., Jin, W.W., An, W., et al., 2020. Oil spill risk assessment for blowout of deepwater drilling platform based on fuzzy bow-tie model. Ship Ocean Eng. 49 (2), 1–5.

Liu, Z.K., Ma, Q., Cai, B.P., et al., 2021. Risk assessment on deepwater drilling well control based on dynamic Bayesian network. Process Saf. Environ. Protect. 149, 643–654. https://doi.org/10.1016/J.PSEP.2021.03.024.

Nhat, D.M., Venkatesan, R., Khan, F., 2020. Data-driven Bayesian network model for early kick detection in industrial drilling process. Process Saf. Environ. Protect. 138, 130–138. https://doi.org/10.1016/j.psep.2020.03.017.

Pan, Y.M., Cao, L., Liu, M., 2021. A PM2.5 concentration prediction method based on LSTM networks. J. Jinling Univ. Sci. Technol. 37 (4), 7–13. https://doi.org/10.16515/j.cnki.32-1722/n.2021.04.002 (in Chinese).

Seraj, S., Delavar, M.R., Rezaee, R., 2021. A hybrid GIS-assisted framework to integrate Dempster–Shafer theory of evidence and fuzzy sets in risk analysis: an application in hydrocarbon exploration. Geocarto Int. 36 (7), 820–838. https://doi.org/10.1080/10106049.2019.1622602.

Shaik, N.B., Pedapati, S.R., Taqvi, S.A.A., et al., 2020. A feed-forward back propagation neural network approach to predict the life condition of crude oil pipeline. Processes 8 (6), 661. https://doi.org/10.3390/pr8060661.

Sheng, Y.N., 2019. Research on Risk Assessment and Control Technology of Drilling Engineering. China University of Petroleum (East China) (in Chinese).

Sheng, Y.N., Guan, Z.C., 2019. Design of drilling engineering risk evaluation and control system and its software development. Oil Dril. Product. Technol. 41 (2), 191–196. https://doi.org/10.13639/j.odpt.2019.02.012 (in Chinese).

Sheng, Y.N., Guan, Z.C., Luo, M., et al., 2019. A quantitative evaluation method of drilling risks based on uncertainty analysis theory. J. China Univ. Petrol. (Ed. Nat. Sci.) 43 (2), 91–96 (in Chinese).

Sheng, Y.N., Guan, Z.C., Zhang, G.H., et al., 2016. Borehole structure optimization based on pre-drill risk assessment. Oil Dril. Product. Technol. 38 (4), 415–421. https://doi.org/10.13639/j.odpt.2016.04.002.

Song, X.Z., Yao, X.Z., Li, G.S., et al., 2022. A novel method to calculate formation pressure based on the LSTM-BP neural network. Petrol. Sci. Bullet. 7 (1), 12–23. https://doi.org/10.3969/j.issn.2096-1693.2022.01.002 (in Chinese).

Sule, I., Imtiaz, S., Khan, F., et al., 2019. Risk analysis of well blowout scenarios during managed pressure drilling operation. J. Petrol. Sci. Eng. 182, 106296. https://doi.org/10.1016/j.petrol.2019.106296.

Theissler, A., Thomas, M., Burch, M., et al., 2022. ConfusionVis: comparative evaluation and selection of multi-class classifiers based on confusion matrices. Knowl. Base Syst. 247, 108651. https://doi.org/10.1016/j.knosys.2022.108651.

Unrau, S., Torrione, P., 2017. Adaptive real-time machine learning-based alarm system for influx and loss detection. In: SPE Annual Technical Conference and Exhibition. OnePetro. https://doi.org/10.2118/187155-ms.

Wang, J., Cao, J.X., Liu, Z.G., et al., 2020. Method of well logging prediction prior to well drilling based on long short-term memory recurrent neural network. J. Chengdu Univ. Technol. (Sci. Technol. Ed.) 47 (2), 227–236. https://doi.org/10.3969/j.issn.1671-9727.2020.02.11 (in Chinese).

Wang, X.G., Li, D.C., 2014. A method of accessing point randomly in a bounded closed region and its realization with mathematica software. J. Yangzhou Polytechnic College 18 (2), 48–50. https://doi.org/10.3969/j.issn.1008-3693.2014.02.013 (in Chinese).

Wang, Y.B., Yang, P., Li, J., et al., 2012. Application of sequential guassian simulation in the KK oilfield of Nigeria. Comput. Era (5), 13–15. https://doi.org/10.3969/j.issn.1006-8228.2012.05.005 (in Chinese).

Wang, Y., Jia, Y., Tian, Y., et al., 2022. Deep reinforcement learning with the confusion-matrix-based dynamic reward function for customer credit scoring. Expert Syst. Appl. 200, 117013. https://doi.org/10.1016/J.ESWA.2022.117013.

Wei, K., Guan, Z.C., Liao, H.L., et al., 2013a. Assessment method of borehole instability risk. J. China Univ. Petrol. (Ed. Nat. Sci.) 37 (2), 62–66. https://doi.org/10.3969/j.issn.1673-5005.2013.02.010 (in Chinese).

Wei, K., Guan, Z.C., Wei, J.H., et al., 2013b. Drilling engineering risk assessment method based on neural network and Monte-Carlo simulation. China Saf. Sci. J. 23 (2), 123–128. https://doi.org/10.16265/j.cnki.issn1003-3033.2013.02.016 (in Chinese).

Wu, Y.L., 2020. Geomechanical parameters and in-situ stress in A block, Xushen gasfield, Songliao Basin. Nat. Gas Explorat. Dev. 43 (3), 54–63. https://doi.org/10.12055/gaskk.issn.1673-3177.2020.03.007 (in Chinese).

Xie, P., Jiang, L.W., Zhao, Y., et al., 2018. Research on real-time prediction and analysis based on neural network for well kick and lost circulation. Mod. Comput. (11), 23–28. https://doi.org/10.3969/j.issn.1007-1423.2018.11.005 (in Chinese).

Xu, G.C., Zhong, G.H., Xie, B., et al., 2014. Evaluation method of shale brittleness logging based on rock physics experiment. Nat. Gas. Ind. 34 (12), 38–45.

Yao, D.C., Ye, J.J., Cui, W., et al., 2015. Study on risk assessment of drilling blowout accident based on fault tree analysis. Drill. Prod. Technol. 38 (5), 12–14+6. https://doi.org/10.3969/J.ISSN.1006-768X.2015.05.04 (in Chinese).

Yi, M., Huang, Z.Q., Zhang, J.H., et al., 2021. Three-dimensional geomechanical modeling of gaoquan structure along the southern margin of the junggar basin and its application to the risk evaluation of deep exploration wells. Oil Dril. Product. Technol. 43 (1), 21–28. https://doi.org/10.13639/j.odpt.2021.01.004 (in Chinese).

Zhang, D.X., Chen, Y.T., Meng, J., 2018. Synthetic well logs generation via recurrent neural networks. Petrol. Explor. Dev. 45 (4), 598–607. https://doi.org/10.11698/PED.2018.04.06 (in Chinese).

Zhang, X., Tian, Y.Y., Han, Z., et al., 2022. Research on lost circulation prediction and diagnosis theoretical model based on machine learning algorithm. Dril. Eng. 49 (2), 58–66. https://doi.org/10.12143/j.ztgc.2022.02.008 (in Chinese).

Zhang, Y.D., Peng, J.Y., Hao, L.Y., et al., 2012. Time-depth conversion difficulties and technical countermeasures for overseas deepwater and complex geological conditions. Prog. Geophys. 27 (4), 1484–1492. https://doi.org/10.6038/j.issn.1004-2903.2012.04.023 (in Chinese).

Zhao, C.L., Yin, H.M., Wang, B., et al., 2019. Risk assessment of drilling site operation based on the structural equation and Monte Carlo Method. Nat. Gas. Ind. 39 (2), 84–93. https://doi.org/10.3787/j.issn.1000-0976.2019.02.012 (in Chinese).

Zhao, Y.F., Hua, Q.X., Chen, J., 2011. Comparison of kriging interpolation with conditional sequential Gaussian simulation in principles and case analysis of their application in study on soil spatial variation. Acta Pedol. Sin. 48 (4), 856–862 (in Chinese).

Zhou, H., Wu, Z.Y., Zhang, X., et al., 2021. Shear wave prediction method based on LSTM recurrent neural network. Fault-Block Oil Gas Field 28 (6), 829–834. https://doi.org/10.6056/dkyqt202106020 (in Chinese).

Zinke, R., Melnychuk, J., Köhler, F., et al., 2020. Quantitative risk assessment of emissions from external floating roof tanks during normal operation and in case of damages using Bayesian Networks. Reliab. Eng. Syst. Saf. 197, 106826. https://doi.org/10.1016/j.ress.2020.106826.